
Masters Theses

Student Theses and Dissertations

Fall 2003

Novel concepts for monitoring the stability of open pit mine highwalls using radar interferometry and spectral imaging

Jami Girard Dwyer

Follow this and additional works at: https://scholarsmine.mst.edu/masters_theses



Part of the [Mining Engineering Commons](#)

Department:

Recommended Citation

Dwyer, Jami Girard, "Novel concepts for monitoring the stability of open pit mine highwalls using radar interferometry and spectral imaging" (2003). *Masters Theses*. 2302.

https://scholarsmine.mst.edu/masters_theses/2302

This thesis is brought to you by Scholars' Mine, a service of the Missouri S&T Library and Learning Resources. This work is protected by U. S. Copyright Law. Unauthorized use including reproduction for redistribution requires the permission of the copyright holder. For more information, please contact scholarsmine@mst.edu.

THESIS
T 8213

NOVEL CONCEPTS FOR MONITORING THE STABILITY OF OPEN PIT MINE
HIGHWALLS USING RADAR INTERFEROMETRY
AND SPECTRAL IMAGING

by

Jami Girard Dwyer

A THESIS

Presented to the Faculty of the Graduate School of the

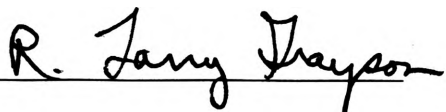
UNIVERSITY OF MISSOURI – ROLLA

In Partial Fulfillment of the Requirements for the Degree

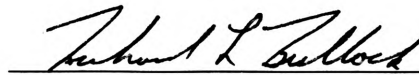
MASTER OF SCIENCE IN MINING ENGINEERING

2003

Approved by:



Dr. R. Larry Grayson, Advisor



Dr. Richard L. Bullock



Dr. David G. Spurlock

**This work was prepared by a U.S. Government employee
as part of official duties and legally may not be copyrighted
in the United States of America.**

**Disclaimer: Any mention of company trade names or
products does not constitute endorsement by the
National Institute for Occupational Safety and Health,
or the Centers for Disease Control and Prevention.**

ABSTRACT

Ground control problems at surface mining operations can occur for a variety of reasons. The geologic setting, rock strengths, joint spacing, orientation, pore pressures, and many other factors contribute to slope instabilities that range from small rock falls to massive slides of material. While much of this ground movement can be predicted or controlled, each year many completely unexpected failures occur. This poses serious safety and economic issues for the mining industry, since any unanticipated movement of the ground increases the potential for significant property damage, injuries, and even death. In the United States alone, 70 people died in slope failure accidents at active mine sites between 1978 and 2000. Obviously, better methods for slope monitoring and mine design are needed to ensure the safety of mine workers.

Standard methods of slope monitoring generally involve measurements at a discrete set of points around the suspected area of instability. Often only a handful of points are monitored over thousands of square feet of highwall exposure. However, complete vigilance to monitor every potential failure block is neither feasible nor economical and is certainly not attainable using common point-displacement monitoring techniques. Many of the current monitoring methods are also difficult to implement at mines where steep highwalls and lack of benches limit access to areas above the working floor. In addition, as mining progresses, it is necessary to monitor different sections of pit walls. Continually relocating devices is not only costly and time consuming, but can also be dangerous, especially on unstable slopes.

This thesis proposes the novel use and potential adaptation of interferometric synthetic radar (INSAR) and multi-spectral imaging to slope monitoring and design. Since the equipment in question is not yet commercially available, field tests were performed to the best extent possible using two prototype systems. The first half of the study describes several geotechnical applications of radar interferometry and discusses the results of limited field trials of a ground-based system. The second portion of the study examines the application of multi-spectral imaging and presents the results from field tests of a prototype instrument used to map the geology of an open-pit mine highwall.

ACKNOWLEDGMENTS

This work would not have been possible without the support of many organizations and individuals. The author gratefully acknowledges the following:

- The funding and project support provided by the National Institute for Occupational Safety and Health (NIOSH), Spokane Research Laboratory. In particular, Mr. Ros Hill, Mr. Ed McHugh, Mr. Ron Mayerle, Dr. Lew Wade, Mr. Kenneth Hay, Mr. Thomas M. Brady, Dr. Jeffrey K. Whyatt, Dr. R. Karl Zipf, Jr., and Mr. Mike Jenkins.
- The funding and opportunities provided by the Department of Mining Engineering, University of Missouri-Rolla (UMR), and Mr. Kent Coman (UMR alumnus).
- The exceptional guidance, support, and advice provided by my advisor, Dr. R. Larry Grayson.
- Dr. Richard L. Bullock and Dr. David G. Spurlock (UMR) for taking the time to participate on this thesis committee.
- The field tests, equipment loans, and technical consultation provided by Dr. Charles Sabine (GeoPix); Dr. Louis Denes, Dr. Milton Gottlieb, and Dr. Boris Kaminsky (Carnegie Mellon Research Institute); and Dr. David Long and Dr. David Arnold (Brigham Young University Microwave Earth Remote Sensing Laboratory) and their graduate students.
- Site access and ore samples provided by various mining companies.
- Editorial, graphics, and administrative support from Barbara Robertson (UMR); Priscilla Wopat, Florence Wilder, Ken Strunk, Linda Noel, and Le Harnasch (NIOSH).
- Finally, I thank my husband, Donald Dwyer, as well as my colleagues Dr. Thomas Camm and Jeffrey Johnson, for motivation to finish and for their remarkable support.

TABLE OF CONTENTS

	Page
ABSTRACT	iii
ACKNOWLEDGMENTS	iv
LIST OF ILLUSTRATIONS	vii
LIST OF TABLES	x
LIST OF ACRONYMS	xi
LIST OF ABBREVIATIONS/UNITS OF MEASURE	xii
1. INTRODUCTION	1
1.1 OVERVIEW OF PROBLEM	1
1.1.1 Review of Mine Safety Statistics	1
1.1.2 Causes of Highwall Instability	2
1.1.3 Highwall Monitoring Systems	3
1.2 OBJECTIVE OF RESEARCH	4
1.3 SCOPE OF STUDY	4
1.4 ORGANIZATION OF MATERIAL	5
2. LITERATURE REVIEW	6
2.1 LIMITATIONS OF COMMONLY USED SLOPE MONITORING SYSTEMS	6
2.2 PROPOSED SYSTEMS	9
2.2.1 Radar	10
2.2.1.1 Specialized Radar Systems—SAR and InSAR	10
2.2.1.2 Evolution of Radar	11
2.2.1.3 Applications of Radar Interferometry and SAR	12
2.2.1.4 Proposed Application of Radar Interferometry to Mine Highwall Monitoring	15

LIST OF ILLUSTRATIONS

	Page
Figure 1. Example of an under-sampled monitoring area	8
Figure 2. Displacement map of Earth’s surface generated by InSAR data.....	14
Figure 3. Spectral signature of kaolinite, a clay mineral.....	18
Figure 4. Spectral signature of azurite, a mineral typically associated with copper deposits.....	19
Figure 5. Field-portable point spectrometer	21
Figure 6. Example of mineral map created from hyperspectral data	23
Figure 7. Basic schematic of BYU’s proto-type radar operation.....	25
Figure 8. Drill cab crushed and operator fatally injured from highwall failure at open pit mine	26
Figure 9. Principles of operation of the radar highwall monitor developed by Australian researchers	27
Figure 10. Principles of operation of BYU radar applied to highwall monitoring.....	28
Figure 11. View of field experiment site for BYU radar	29
Figure 12a. View of the experimental site. Gravel pile used to simulate a mine highwall.....	30
Figure 12b. View of test target from the radar instrument location.	31

Figure 13. CMRI's spectro-polarimetric imager in protective housing (above), internal components (at right)	32
Figure 14. Image cube formed by accumulation of spectral data	34
Figure 15. Original images from CMRI spectro-polarimetric imager: a) drill core; b) vegetation and outcrop; c) hand samples; and d) wall in main pit.	35
Figure 16. Laboratory calibration a.) hand specimen that was used to calibrate the CMRI imager; b) image from CMRI spectrometer on sample and larger specimen.....	36
Figure 17. CMRI imager results versus ASD point spectrometer	37
Figure 18. Baseline radar readings for each radar antenna	38
Figure 19. Large displacements in known directions were recorded as a person climbed up and down the gravel slope within the radar scene	39
Figure 20. Raw data from each radar receiver during climbing tests	40
Figure 21. Radar phase difference data of person walking down gravel slope	41
Figure 22. Box indicates analysis region	43
Figure 23. Enlarged view of study area indicated in Figure 22	44
Figure 24. Net displacement for each adjacent pixel pair along the sample line indicated in Figure 23	46
Figure 25. Data analysis along the slope profile at three separate times	47

Figure 26. Results of displacement along slope profile at times $t = 10$ sec (before person walked through radar path), $t = 22$ sec (as person walked through radar path), and $t = 28$ sec (after slope has begun to stabilize).....	48
Figure 27. A displacement map could be generated by comparing phase difference information from two separate radar views of the highwall recorded at different times.	49
Figure 28. Mine highwall at the test site. Study area is outlined	52
Figure 29. Diagnostic spectral signature of one of the minerals present at the field test site.....	53
Figure 30. Comparison of spectral data	54
Figure 31. Spectral profiles of ore match with diagnostic absorption features.....	55
Figure 32. Results from the CMRI spectro-polarimetric imager. Blue areas correspond to ore; green areas to waste; and black to unclassified spectra.....	56

LIST OF TABLES

	Page
Table 1. Partial list of currently operating airborne hyperspectral imagers.....	20
Table 2. Partial list of currently available point/field spectrometers	21
Table 3. CMRI spectro-polarimetric imager instrument specifications.....	33

LIST OF ACRONYMS

ASD	Analytical Spectral Devices
BYU	Brigham Young University
CMRI	Carnegie Mellon Research Institute
EDM	Electronic Distance Measurement
GPS	Global Positioning System
IFSAR	Common variation of INSAR, Interferometric Synthetic Aperture Radar
InSAR	Interferometric Synthetic Aperture Radar, also referred to as IFSAR
MERS	Microwave Earth Remote Sensing Laboratory, at Brigham Young University
MSHA	Mine Safety and Health Administration
NASA	National Aeronautics and Space Administration
NIOSH	National Institute for Occupational Safety and Health
RF	Radio frequency
SAR	Synthetic Aperture Radar
SRL	Spokane Research Laboratory, a NIOSH facility
USGS	United States Geological Survey
YINSAR	Name of BYU's proto-type interferometric synthetic aperture radar.

LIST OF ABBREVIATIONS—UNITS OF MEASURE

cm	centimeters
ft	feet
m	meters
nm	nanometers (10^{-9})
μm	micrometers (10^{-6})
GHz	gigahertz (10^9)
Hz	hertz
in	inches
km	kilometer
MHz	megahertz (10^6)
sec	seconds
t	time

1. INTRODUCTION

1.1 OVERVIEW OF PROBLEM

1.1.1 Review of Mine Safety Statistics. Whether on the surface or underground, any unanticipated movement of the ground at a mining operation can generate hazardous conditions that could lead to endangerment of lives, demolition of equipment, and the loss of property. While there is a general knowledge that ground failures in underground mines are dangerous, many people fail to realize that rock falls, material sloughs, or highwall failures in surface mines can also have catastrophic consequences. For example, in 2001, 10 miners were killed when a slope failure occurred at the Nchanga Mine in Zambia (Esipusu, 2001). Even the smallest of failures can be dangerous and cause significant problems if benches that support main haul roads fail or if facilities are threatened by displacement of the rock mass. Failure to scale highwalls adequately at quarries can also have devastating consequences, as can be seen from the following excerpts of these recent Mine Safety and Health Administration (MSHA) fatal accident investigation reports:

- [A] rock found near the victim ... measured about 4 by 4 by 3 inches and weighed 2 pounds, 13 ounces.” (1999a)
- A rock fell from the quarry wall striking the victim, causing fatal injuries. ... Death was attributed to head trauma. ... The rock or rocks that struck the victim could not be identified, nor could it be determined from what height they fell from the highwall. (1999b)

In the United States, a review of MSHA data indicates that 765 accidents involving falls of face or highwall in the period from 1978 through 2000 (McHugh, 2002; MSHA, 2000). Of these, 70 were fatal and five caused permanent disabilities, which is

an average of 33 failures and three fatalities per year. Obviously, better methods of monitoring highwalls and designing slopes are needed to ensure the safety of mine workers. As such, the National Institute for Occupational Safety and Health (NIOSH), Spokane Research Laboratory (SRL), has provided funding to study mine slope stability accidents in order to reduce the hazards associated with highwall failures.

1.1.2 Causes of Highwall Instability. There are several ways to reduce the chances of surface ground control accidents. First, geotechnical designs should be engineered with an adequate factor of safety. This requires an in-depth understanding of mine geology, rock mass properties, and hydrogeologic factors. Controlling costs in mining is imperative, especially in times of low and/or fluctuating commodity prices. Often pit walls are made as steep as possible to minimize waste removal and surface disturbance, and to maximize ore recovery. The tradeoff is a decreased margin of safety, since steeper walls can compromise stability.

Secondly, poor blasting practices can induce back-break and unnecessary fracturing of the highwall. While these fractures may not cause immediate problems, unintended cracks in the benches and walls provide pathways for water. The buoyant forces of water, freeze/thaw cycles, and increased weathering can decrease effective joint strengths and cause failures. Where applicable, benches, mechanical rock fall catchment systems, or secondary supports may alleviate problems associated with rocks falling to the working floor.

However, even the most carefully designed slopes may fail because of unknown geologic structures, unexpected weather changes, seismic shock, or other factors. While geotechnical designs and certain support systems may enhance overall rock mass

strength, diligent monitoring and examination of slopes for early warning signs of failure are the most important means of protecting exposed mine workers.

1.1.3 Highwall Monitoring Systems. The instruments selected for a slope-monitoring program depend on the particular situation to be monitored. A comprehensive monitoring system may include instruments capable of measuring surface and subsurface rock mass displacement, groundwater parameters, and blast vibration levels. The majority of these instruments only provide information about a single location. Often, a mere handful of points are monitored over thousands of square feet of highwall exposure. If an inadequate number of instruments are used, or if the instruments are not located in crucial areas, the possibility exists that the early indications of a slope failure would go undetected.

Constant vigilance to monitor every potential failure block is neither feasible nor economical and is certainly not attainable using existing point-monitoring systems. Recent developments in instruments, such as prismless laser range finders, partially address the problem of under-sampling large areas for movement. However, the range and accuracy of these units can vary greatly depending on the reflectivity of the rock, the angle of the rock face, weather, and other factors. Many of the current monitoring methods are also difficult to implement at quarries and surface coal mines, where steep highwalls and lack of benches limit access to areas above the working floor. In addition, as mining progresses, monitoring different sections of the pit walls becomes necessary. Continually relocating devices is not only costly and time consuming, but can also be dangerous, especially on unstable slopes.

1.2 OBJECTIVE OF RESEARCH

The objective of this research is to explore new methods of slope monitoring that would overcome the limitations of current point-displacement systems. Tests of two currently existing remote-sensing technologies will be analyzed to determine the feasibility of modifying and adapting them for use as novel mine highwall monitoring methods. The two technologies that will be examined are interferometric synthetic aperture radar (InSAR) and multi-spectral imaging.

1.3 SCOPE OF STUDY

To date, most remote sensing applications, such as spectral imaging and InSAR, have been applied using satellites or other sophisticated airborne platforms. Only recently have increased microprocessor speeds, data storage capacities, signal processing capabilities, and other computer advances led to the development of smaller, portable, ground-based systems. Unfortunately, much of the technology in the latter category is still in the early stages of research and development. Through NIOSH, a proposal for field trials of InSAR and spectral imaging as slope monitoring tools was funded. However, at the time of the tests, ground-based versions of the instruments were not commercially available, and construction of such instruments was not economic for the purposes of the project. Therefore, cooperative agreements were established with two external research facilities to provide prototype equipment and support. The Microwave Earth Remote Sensing Laboratory at Brigham Young University (BYU) in Sandy, Utah, furnished the prototype InSAR instrumentation, and the Carnegie Mellon Research Institute (CMRI) in Pittsburgh, Pennsylvania, furnished a prototype spectro-polarimetric

imager. Each prototype instrument was field tested to assess the feasibility of using this technology to monitor open-pit highwalls.

1.4 ORGANIZATION OF MATERIAL

Each of the following chapters is divided into two major subsections related to two separate technologies—interferometric radar and spectral imaging. Both technologies are proposed as novel methods for monitoring the stability of open-pit mine highwalls.

Chapter 2 introduces current monitoring system limitations and presents the rationale for developing a new type of monitoring system employing radar interferometry and/or spectral imaging. An extensive literature search provides background information on the evolution of each technology, and a number of recent successful applications in the field of geosciences are highlighted.

Chapter 3 provides detailed system specifications and principles of operation for the prototype instruments tested throughout the course of this research. An overview of the field site locations and experimental procedures is also presented.

Chapter 4 discusses the results from the prototype radar instrument and prototype spectral imager. Limitations of the field tests are described as well as the problems encountered during testing.

Chapter 5 summarizes the field experiments and suggests directions for future research and development.

2. LITERATURE REVIEW

This chapter provides background information related to the limitations of current, commonly used slope monitoring systems. A new type of remote-sensing approach that uses multi-spectral imaging and radar interferometry to overcome these limitations is proposed. An introduction to the basic principles of operation is included, and an extensive literature review summarizes successful airborne InSAR and hyperspectral applications. Based on the history and development of the proposed systems, the rationale for developing a ground-based system for slope monitoring is highlighted along with recent related research.

2.1 LIMITATIONS OF COMMONLY USED SLOPE MONITORING SYSTEMS

The types of instruments selected for a slope-monitoring program depend on the particular problems to be monitored. A comprehensive monitoring system may include instruments capable of measuring surface and subsurface rock mass displacement, groundwater parameters, and blast vibration levels. Common instruments include electronic distance measurement (EDM) surveying equipment, laser range finders, global positioning system (GPS) instruments, crack gages, extensometers, inclinometers, piezometers, and tiltmeters. A description of the full realm of available instrumentation is not within the scope of this thesis. Readers requiring more information about current practices related to monitoring strategies, equipment, and specifications can find excellent overviews in Kliche, 1999; Abramson et al., 1996; Szwedzicki, 1993; Call and Savely, 1990; and CANMET, 1977. Specific information on blast vibration monitoring

and damage control techniques can be found in Cunningham, 2001; Hustrulid, 1999; Scott, 1996; and Oriard, 1972.

One of the most common systems for monitoring slope movement is a survey network. Survey networks use electronic distance measurement (EDM) equipment, a series of target prisms placed on and around areas of anticipated instability, and one or more nonmoving control points for survey stations. The angles and distances from the survey station to the prisms are measured on a regular basis to establish a history of movement. The surveys can be done manually by a survey crew or can be automated. Surveying equipment can detect both very small and very large earth movements; however, information is gathered only at the points where the prisms are installed.

Figure 1 is an illustration of a difficult situation that could arise with respect to highwall monitoring. In the figure, the dots represent a mock-up of monitoring prism placements. For this example, because of the enormous surface area of this mine, it is conceivable that a monitoring system might have missed the failure entirely if the target prisms had been configured as shown. Fortunately, this particular mine site was well monitored, and while the costs of clean up were considerable, no lives were endangered.

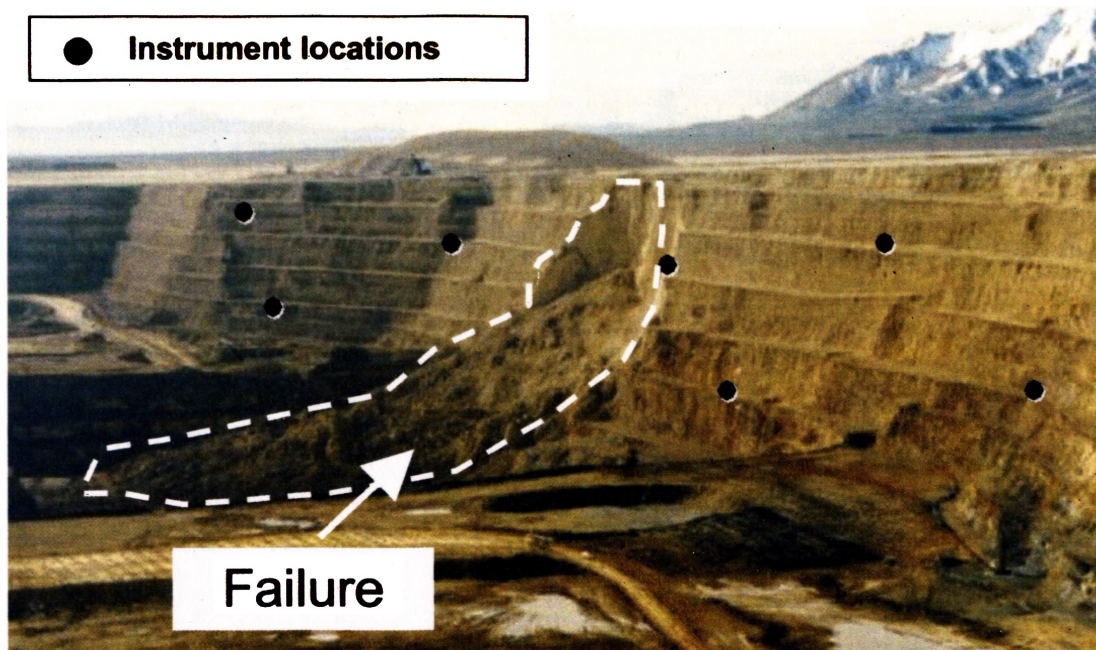


Figure 1. Example of an under-sampled monitoring area.

Since the majority of common slope-monitoring instruments only provide information about a single point, the installation of numerous instruments may be necessary to fully evaluate the extent of a slope or highwall hazard. However, financial and practical limits dictate the number of instruments that can be installed. Prices for such equipment range from a few hundred to thousands of dollars apiece. In addition, collecting and analyzing data from manual monitoring systems can be very time consuming. An increase in the number of instruments may translate into increased manpower requirements. Automated systems, radio links, data transmission, and data storage capabilities allow more data to be collected using fewer personnel and allow for around-the-clock measurements. However, increasing the sophistication of a system will

incur additional costs, and the mine personnel may require extensive technical training in order to calibrate and maintain complex electronic systems.

Another potential problem is that manual equipment might only be read sporadically and often only during the day. Crucial warning signs of slope instability that occur during the dark of night may go unnoticed until daylight. Even with some automated systems, data analyses are only performed during the day when the engineering and surveying staff are onsite.

To overcome the many limitations of common slope monitoring equipment, a new type of monitoring system is needed that can provide reliable information about the entire highwall (not just select points), 24-hours per day. Ideally this system would be based on remote-sensing principles, thereby eliminating the need to send personnel into potentially unstable areas to install monitoring equipment. Remote sensing would also allow monitoring of areas that were otherwise inaccessible, and since no instrumentation would physically be required on the highwall, the probability of losing expensive instruments in a slope failure would be reduced. Displacement data coupled with detailed geologic information would supply geotechnical engineers with better information for designing slopes and would hopefully decrease hazards to mine workers.

2.2 PROPOSED SYSTEMS

The objective of this research was to explore new methods of slope monitoring that would overcome the limitations of point-based displacement systems. Tests of two existing remote-sensing technologies were analyzed to determine the feasibility of modifying and adapting them for use as novel mine highwall monitoring methods. The first proposed system, based on radar principles, would be used to track displacements of

unstable material. The second system, spectral imaging, would provide information about the highwall geology.

2.2.1 Radar. Radar (radio detection and ranging) is a type of active, remote-sensing system that sends and receives electromagnetic radiation in the form of radio waves or microwaves. The four basic components of radar include: 1) a transmitter that transmits pulses of energy; 2) a receiver that accepts reflected signals; 3) an antenna or antenna array that transmits a narrow beam of energy; and 4) a recorder that records or processes the information (Campbell, 1996). Radar works by transmitting an electromagnetic signal through an antenna toward an object. When this signal reaches the object, a portion of the energy is returned to the receiver as an echo. By analyzing the signal from the echo, information regarding the object can be determined. For example, radar systems are capable of measuring the distance to a target by determining the time it takes for a transmitted signal to be returned.

2.2.1.1 Specialized Radar System — SAR and InSAR. Synthetic Aperture Radar (SAR) is a specialized type of high-resolution, ground-mapping radar originally designed to operate from aircraft and satellites. The term “synthetic” is used to describe how SAR uses the movement of an aircraft or a satellite to replicate a long antenna. Measurements are taken repeatedly from different positions along a flight path, and the receiver processes the signals as if the information was obtained from one long antenna instead of from several smaller ones. This allows the radar to achieve higher resolutions than standard radar. Detailed information on radar imaging and SAR principles of operation can be found in Curlander & McDonough, 1991; Lunetta & Elvidge, 1998; Henderson and Lewis, 1998; and Elachi, 1988. SAR can be used to measure topography,

track changes, and detect disturbances of the earth's surface. A variation of SAR—Interferometric Synthetic Aperture Radar (also commonly referred to as InSAR, IFSAR, or DiffSAR)—compares subsequent radar measurements made over the same region. In principle, if two radar images are taken from exactly the same position, but at different times, the resulting images should be identical. However, if there has been any change of the ground, this difference will appear as interference patterns on subsequent radar images. The differences in the measurements, i.e., the radar interferograms, can be used to derive information about surface topography, topographic change, or displacement over time.

Most radar interferometry research has been developed in relation to SAR, which requires a moving platform such as an aircraft or spacecraft to pass over the same region with two or more flight passes. At present, there are a number of space-borne SAR systems from Europe, Canada, Japan, and the United States that routinely collect data for a variety of earth science applications. Radar interferometry can also be performed from a stationary, ground-based position. This principle is the basis of the proposed highwall monitoring system that is discussed further in later chapters.

2.2.1.2 Evolution of Radar. Radar research began in the late 1890's after Heinrich Hertz proved the existence of radio waves as originally proposed by James Maxwell in the 1860's. Shortly thereafter, scientists discovered that radio waves were blocked and reflected back to the transmitter by objects in the radio wave path. In one of the first applications of radar, the military used the systems to warn of intruding ships in protected waterways. Then, in 1904, Christian Hülsmeyer was awarded one of the first radar patents for a collision-avoidance system that could be mounted on ships.

Hülsmeier's system had a range of approximately one mile (1.6 km); longer range radars began to appear by the 1920's. However, most of the considerable advances in radar technology were developed during World War II, the majority of which were classified and military in nature. Geoscience applications using radar were not extensively found in the published literature until the 1960's when the government de-classified certain sets of radar data (Henderson and Lewis, 1998). Additional data were made available to the public from new airborne missions by the National Aeronautics and Space Administration (NASA) in the late 1960's and early 1970's and led to the discovery of many geoscience applications for radar.

2.2.1.3 Applications of Radar Interferometry and SAR. Even though radar technology has been in use for nearly a century, wide-spread application to the geosciences is a fairly recent development. One of the first reported applications of remote-sensing interferometric radar involved imaging the surface of Venus (Rosen et al., 2000; Rogers and Ingalls, 1969). The first report of an InSAR observation of Earth was reported by Graham (1974). These early studies paved the way for the first airborne systems capable of constructing surface topography (Li and Goldstein, 1990; Goldstein et al., 1988; and, Zebker and Goldstein, 1986).

Additional research determined that once the topographic component of a scene is established, subsequent radar images of the same scene can be compared temporally. This is generally referred to as "differential interferometric SAR" and is used to derive detailed information about surface displacement and velocity. The first proof of this concept was discovered when data from a satellite InSAR system showed minute elevation changes in soil before and after irrigation of a field (Gabriel et al., 1989).

However, it was not until 1992 that the earth science community took substantial note of this development and obtained independent ground-based verification of the results. In 1992, data collected by the European Remote-Sensing Satellite (ERS-1) were used to generate displacement maps illustrating the net movement of the Earth's surface as a result of the large (Richter magnitude 7.2) Lander's earthquake in southern California. InSAR measurements of displacement were shown to correlate with ground-truth information from sensors placed along regional geologic faults (Massonnet et al., 1993). Around the same time, another study used ERS-1 InSAR data to estimate ice-stream velocity in Antarctica (Goldstein et al., 1993).

These pioneering studies of tectonic motion and ice flow generated enormous interest in the geosciences community because they pointed to an entirely new way to study the surface of the Earth. From the mid-1990's until the present time, InSAR technology has advanced rapidly and numerous studies using airborne InSAR have been undertaken to study ground movement. Several additional InSAR investigations of seismic displacement have been published (Rosen et al., 1998; Ozawa et al., 1997; Clarke et al., 1997; Massonnet et al., 1995a, 1994; Meyer et al., 1995; Peltzer and Rosen, 1995; and, Peltzer et al., 1994). Other ground displacement applications have included: (1) observing volcanic motion (Wicks et al., 2002; Froger et al., 2001; Lu et al., 2000, 1997; Lanari et al., 1998; Briole et al., 1997; Thatcher and Massonnet, 1997; Rosen et al., 1996; Massonnet et al., 1995a; Mouginiis-Mark, 1994a, 1994b; and, Mouginiis-Mark and Garbeil, 1993); (2) monitoring displacement of unstable slopes and landslides (Berardino et al., 2003; Colesanti et al., 2003; Tarchi et al., 2003; Carnec et al., 1996; Fruneau and Achache, 1996a; Fruneau et al., 1996b; and, Mantovani et al., 1996;); and, (3) studying

subsidence resulting from the extraction of ground water, minerals, or petroleum products (Cox, 2001; Hoffmann et al., 2001; Stancliffe and van der Kooij, 2001; Carnec and Delacourt, 2000; Amelung et al., 1999; Fielding et al., 1998; Galloway et al., 1998; Massonnet et al., 1997; Stow, 1997; De Rouffignac et al., 1995; and, Dixon, 1994). Figure 2 is an example of a displacement map generated using InSAR.

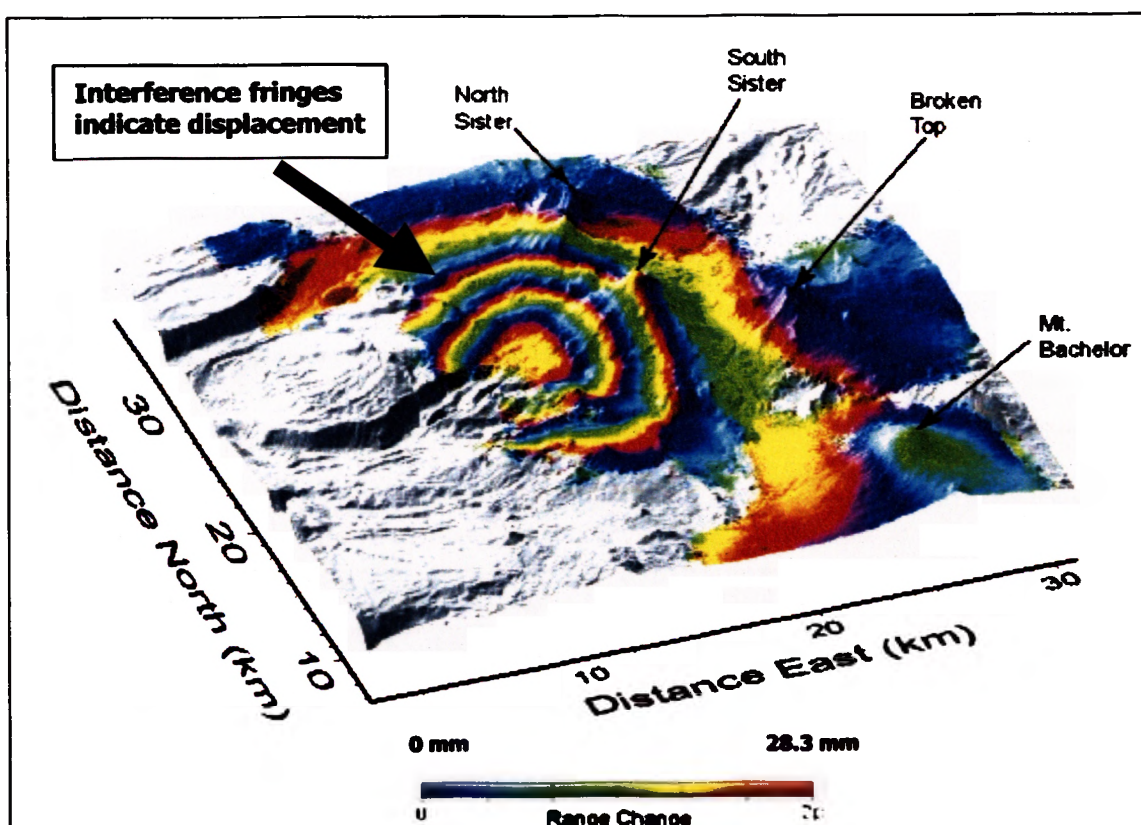


Figure 2. Displacement map of Earth's surface generated by InSAR data. This example shows interference fringes occurring as a result of volcanic activity. Photo courtesy of U.S. Geological Survey (Wicks, 2002). (Above illustration was originally reproduced in color.)

2.2.1.4 Proposed Application of Radar Interferometry to Mine Highwall Monitoring. SAR has many advantages over current types of monitoring systems. The primary advantage of InSAR is that ground displacements can be monitored without the need for installation of physical sensors. Able to work in nearly all weather, InSAR can acquire imagery through fog, mist, rain, haze, or cloud cover, and can operate day or night. Also, InSAR is capable of sampling large areas for ground displacement, which is a tremendous advantage over survey networks, extensometers, and other instruments which sample movement on a discrete set of points.

To date most InSAR applications relied on satellite or other sophisticated airborne platforms. However, the use of airborne or space-borne InSAR data is not practical for day-to-day mining operations due to high costs of data acquisition, and long cycle times for repeat passes of aircraft or satellites. Recently, research and development of smaller, portable, ground-based systems has begun. These systems will be more versatile, and less expensive than traditional airborne InSAR, and will be more practical for a variety of applications. For example, ground-based systems were used recently to monitor movement on a landslide in Italy (Tarchi et al., 2003) and a volcano in France (Malassingne et al., 2001).

Some of the first research and development of a system to monitor mine highwalls began in Australia in 1997 (Reeves et al., 1997). Those tests were reported as successful (Reeves, 2002), and a press release indicated that this instrument was commercially available for short-term lease in June 2002 (University of Queensland, 2002). In the United States, the Microwave Earth Remote Sensing Center at Brigham Young University (BYU) developed a low-cost, compact, InSAR (they named

“YINSAR”) capable of operating from a small aircraft or from the back of a ground-based vehicle (Thompson, 1996-2000). A variation of this instrument was proposed as a means to increase safety for open pit mine workers by detecting early movement on mine highwalls (Girard and McHugh, 2000; Sabine et al., 1999a; and, Girard et al., 1998). With funding from NIOSH, a cooperative agreement was established to modify and test the BYU proto-type instrument for mine safety applications. Detailed information about the instrument and results from the experiments are described in Chapters 3 and 4.

2.2.2 Spectral Imaging. In addition to displacement monitoring, information on geologic structures and weak rock units that have the potential for causing slope instabilities must be incorporated into a highwall monitoring and evaluation program. Current practices for mapping the geology at a mine site are very labor intensive and generally rely on manual mapping by a small number of geologists. Geologic maps can vary greatly in quality and detail due to individual subjectivity and the extreme complexity of many deposits. There are financial and practical limits to the number of samples that can be submitted for geochemical or engineering analyses. Inevitably a large percentage of data shown on geologic maps is subject to scrutiny. Many results are mathematically interpolated or based on conjecture by geologists with a limited number of data points or observations.

Major geologic features are usually well-delineated, but the degree and extent of smaller rock units or structural systems with the potential to cause slope instability may be inadvertently overlooked. A contributing factor in many slope failures is the presence of hydrothermal alteration (clay) in the rock mass (Watters and Delahaut, 1995). The degree of alteration directly affects the rock mass strength, so information about these

weak zones is crucial for stability analyses. Even with an adequate amount of resources available for geologic mapping, the extent of hydrothermal alteration in a rock unit is difficult to accurately estimate by visual inspection alone. In addition, critical portions of the highwall may be inaccessible which makes direct measurement of the rock strength impossible.

In order to address the difficulties and limitations associated with the geologic mapping process, a second system based on spectral imaging is proposed for improving mine slope monitoring. This system would complement the data obtained by traditional geologic mapping methods and would be based on remote sensing principles (much like the aforementioned radar system). This system would provide a means to quantitatively and objectively map the geology of a mine highwall from a distance without the need to send a geologist out on a potentially unstable slope.

2.2.2.1 Principles of Operation of a Spectral Imager. Just as every human has unique fingerprints, the minerals on the earth's surface have a characteristic spectral signature. The manner in which light of different wavelengths is reflected or absorbed by each material is known as the reflectance spectrum and is primarily based upon the chemical composition of the material. By filtering light of specific wavelengths, images can be created that differentiate specific materials. Figures 3 and 4 illustrate examples of the spectral signatures for two randomly selected minerals—kaolinite (a clay mineral) and azurite (a mineral often associated with copper deposits). As can be seen from the figures, the spectral signatures of each mineral are very distinct. A spectrometer is a

device that collects these diagnostic spectral-absorption features (reflectance spectra). Identification of the minerals is then achieved by comparing the data to standardized spectral images such as those found in the spectral library developed by the United States Geological Survey (USGS) (Clark et al., 1993). Certain unique spectral features within a small portion of the total spectrum may be sufficient to confidently identify many minerals.

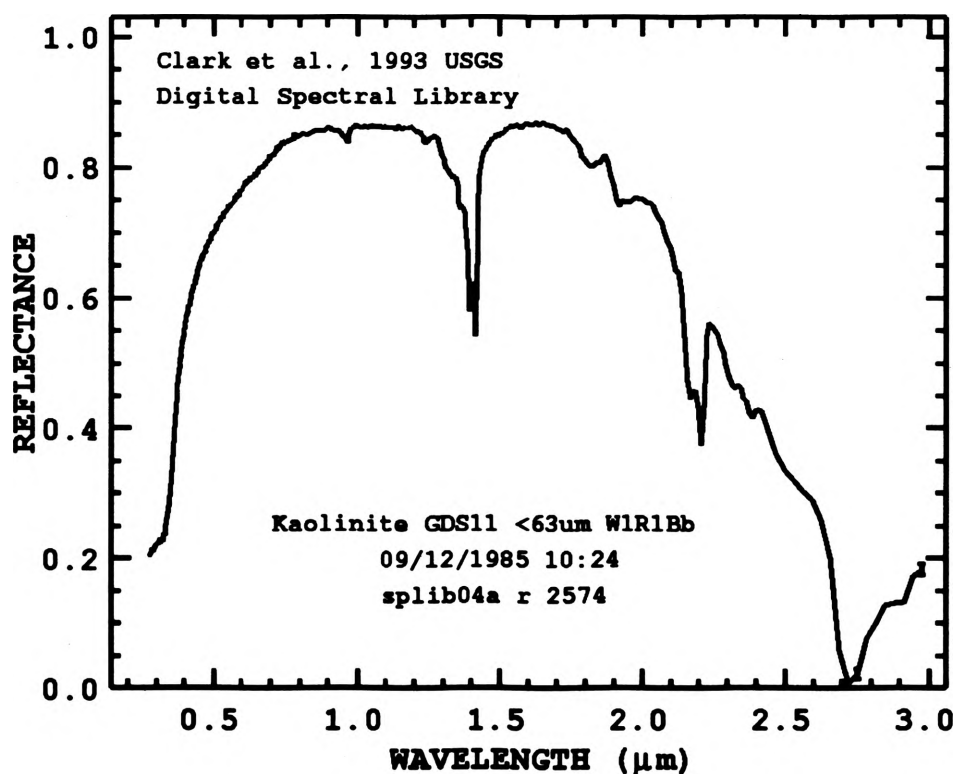


Figure 3. Spectral signature of kaolinite, a clay mineral (Clark et al., 1993).

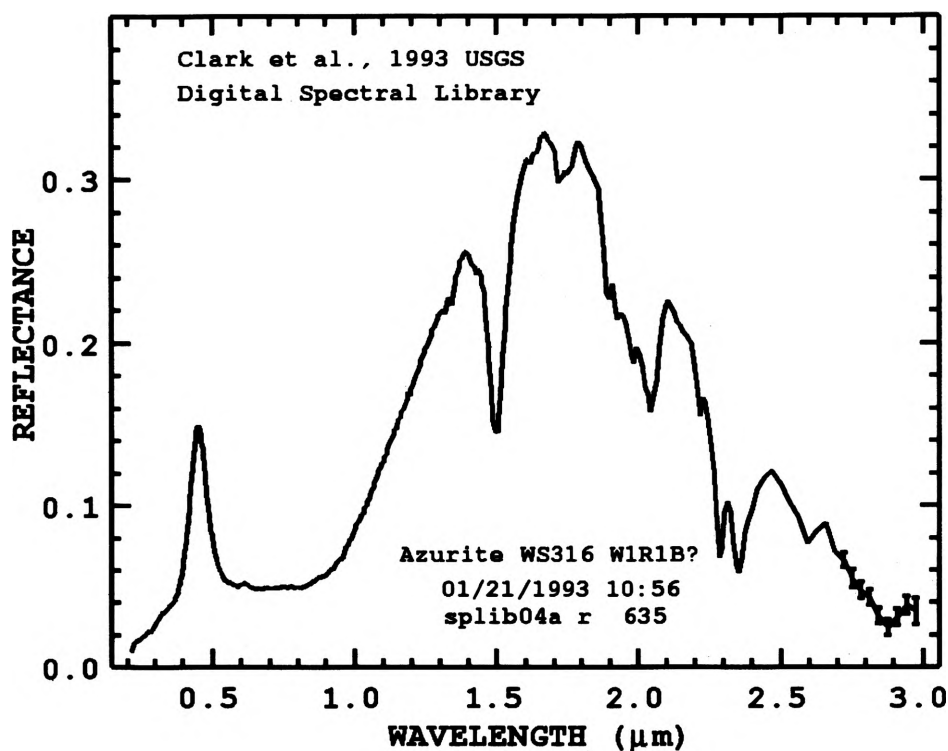


Figure 4. Spectral signature of azurite, a mineral typically associated with copper deposits (Clark et al., 1993).

Much like the radar methods discussed previously, imaging spectroscopy is a relatively new remote-sensing technique with instrumentation and analysis methods primarily developed within the last decade (Clark and Swayze, 1996). As such, the terminology for the field varies between publications and has been referred to as imaging spectroscopy or spectrometry, as well as multi-, ultra-, or hyperspectral imaging. Multi- and hyperspectral imaging are based on a small number (up to hundreds) of narrowly defined spectral channels. Higher resolution ultra-spectral imaging applies primarily to the study of atmospheric gasses. Generally speaking, the prefixes refer to the number of

imaging bands available, but the terms multi- and hyperspectral are often used interchangeably throughout the remote-sensing literature.

To date, most of the spectral imagers have been developed for airborne and satellite operation. One of the first hyperspectral imaging sensors, the airborne imaging spectrometer (AIS), was designed in the early 1980's by NASA's Jet Propulsion Laboratory (Campbell, 1996). The AIS instrument greatly expanded the scope of remote sensing and was followed shortly thereafter by the construction of one of the principle instruments still in use today—the airborne visible infrared imaging spectrometer (AVIRIS). Table 1 lists a few of the currently operating airborne hyperspectral systems.

Table 1. Partial list of currently operating airborne hyperspectral imagers.

Name	Spectral Coverage (nm)	# of Bands	Country of Origin	Available since
Airborne Visible Infrared Imaging Spectrometer (AVIRIS)	380-2500	224	United States	1987
Compact Airborne Spectrographic Imager (CASI-2)	400-1000	288	Canada	1989
Modular Airborne Imaging Spectrometer (MAIS)	440-2500	71	China	1991
Hyperspectral Mapping (HyMAP)	450-2480	126	Australia	1997

In addition to airborne and satellite imagers, several companies also manufacture hand-held, field-portable spectrometers such as the instrument shown in Figure 5.



Figure 5. Field-portable point spectrometer. (Photo courtesy of Integrated Spectronics [Cocks, 2003]).

Table 2 is a list of several currently available field spectrometers manufactured by various companies.

Table 2. Partial list of currently available point/field spectrometers.

Manufacturer	Instrument	Spectral Coverage (nm)
Integrated Spectronics (http://www.intspec.com)	Portable Infrared Mineral Analyser (PIMA)	1300-2500
Geophysical and Environmental Research Corporation (GER) (http://www.ger.com)	GER HI RES	350-2500
Analytical Spectral Devices (ASD) (http://www.asdi.com)	Fieldspec Handheld	350-1075

Field spectrometers are portable and lightweight (approximately 3.5 kg (7.7 lb) including battery packs) and operate on the same principles as airborne imagers. However, field spectrometers are used to collect data from a single, spot reading as opposed to airborne spectrometers which collect data from a compilation of pixels (i.e., an image) over an entire scene. Field spectrometers are frequently used to establish ground-truth for airborne campaigns. Data acquired from both hand-held and airborne spectral imagers are used to support multiple scientific investigations related to oceanography, ecology, hydrology, geosciences, and other fields.

2.2.2.2 Applications of Spectral Imaging. Just as military research of the electromagnetic spectrum in the microwave range advanced the field of radar, military research of the infrared portion of the spectrum laid the groundwork for spectral imaging. Spectral imaging is a powerful mapping tool with current applications ranging from biogeochemistry studies of the ocean (Brown and Podesta, 1997, and Michaels and Seigel, 1996) to tracking and assessing forest fires and fire damage (Asakuma et al., 2002; Barducci et al., 2002; and Roy et al., 2002). Spectral imaging has also been used to image crops and other vegetation to assess the health of the plants and to provide information about the soil beneath the growth. This was one of the earliest civilian applications of remote sensing (Colwell, 1956, as reported in Campbell, 1996). Plants will often absorb trace elements of the minerals within the soil, which will in turn cause a spectral shift. Knowledge of this particular phenomenon has been used as a mineral exploration tool in heavily vegetated areas (Chang and Collins, 1983, and Collins et al., 1983).

Mineral exploration is another one of the earliest and most common applications of airborne hyperspectral imaging. Overviews of remote sensing and exploration are available in Sabins (1999). An elaborate and detailed five-year study of the mineralization around Cuprite, Nevada (Figure 6), formed the basis of the USGS spectral library (Clark et al., 1993). Specific examples of mineral exploration can be found in Asadi and Hale (2001), Sun et al. (2001), King et al. (1995), and Ishiwada et al. (1992).

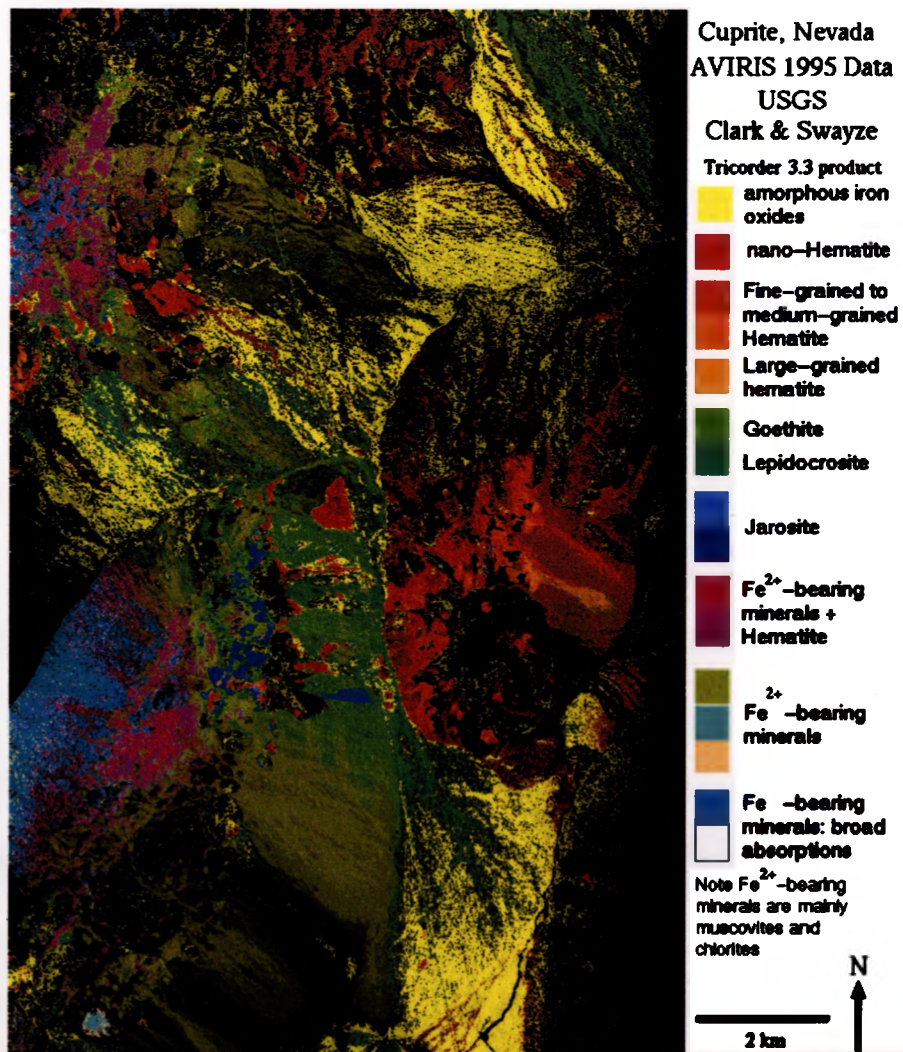


Figure 6. Example of mineral map created from hyperspectral data. (Photo courtesy of USGS [Clark and Swayze, 1996]).

Hyperspectral imaging has also been used in the mining industry for environmental risk assessments and detection of potential sources of surface acid mine drainage. Information from airborne hyperspectral surveys are useful for studying sediment compositions, heavy metal concentrations, and water quality around active and abandoned mine sites (Dalton et al., 2000, and, Swayze et. al., 2000). Data can also be used to locate regions of acid-neutralizing mineral assemblages and to determine the efficacy of mine wastewater treatment facilities (Clark et al., 1998, and King et al., 1995). Airborne spectral systems are useful, extremely efficient, and have shown great success in acquiring data from large areas. However, in order to apply spectral imaging to the problem of mine highwall mapping, a portable, ground-based system is needed.

2.2.2.3 Proposed Application of Spectral Imaging to Mine Highwall Mapping. The use of spectral imaging as an improved method for geologic mapping of mine highwalls would be advantageous for many reasons (Sabine, et al., 1999b). First, spectral identification of minerals would remove the human error and subjectivity of trying to visually determine the degree of alteration in a rock mass. This would enhance the safety of the mine workers since the weak areas of the highwalls could be mapped out quickly and efficiently. Secondly, spectral imaging would provide a means by which workers could map large extents of mine highwalls or inaccessible areas, from a safe distance. Spectral analyses could also be used to define faults, shear zones, fracture systems and other features that degrade the overall strength of the rock mass. All of this information could be integrated into geotechnical designs, mine planning, and mine monitoring systems to improve mine safety and efficiency.

3. EXPERIMENTAL METHODS AND PROCEDURES

3.1 RADAR INTERFEROMETRY

3.1.1 Radar Prototype Specifications. The prototype system developed by Brigham Young University consists of a transmitter, two slotted-waveguide receiver antennas, and an embedded computer. The radar operates at a 9.9 GHz center frequency with a 200 MHz bandwidth. The signals are digitized at 500 MHz, and the pulse repetition frequency is 1200 Hz with the capability to vary pulse lengths from 1 to 150 microseconds (Long, 2003). The computer controls the radar transmitter and receiver, digitizes the receiver outputs, computes the terrain topography, and determines if displacement on the slope has occurred (Figure 7).

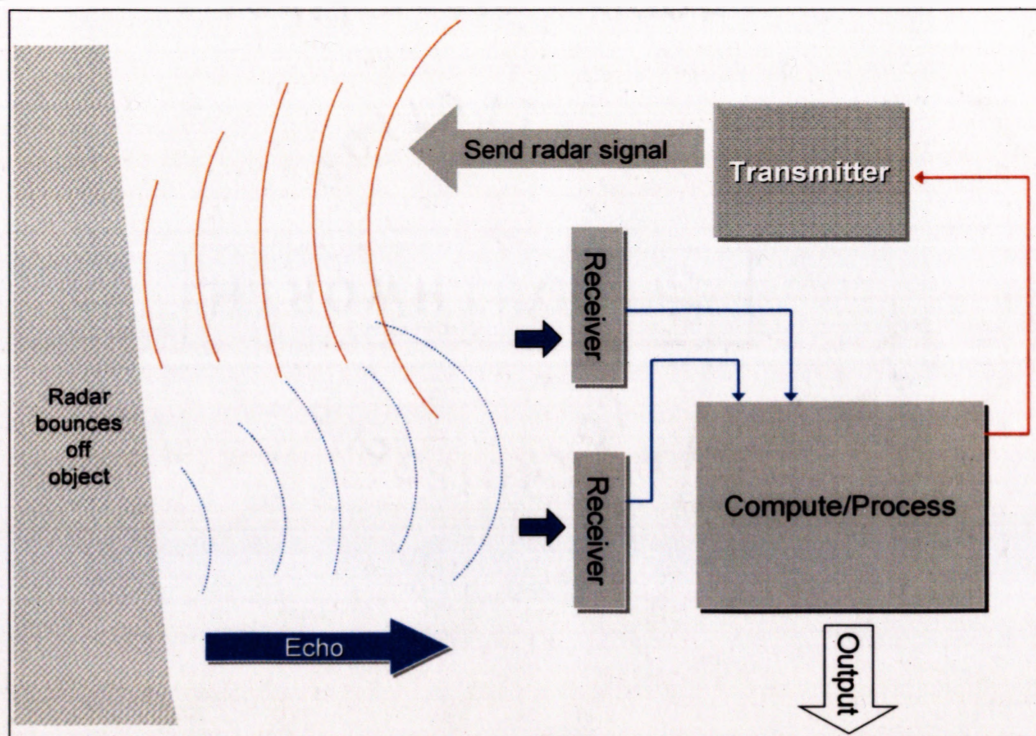


Figure 7. Basic schematic of BYU's proto-type radar operation.

3.1.2 Prototype Principles of Operation. The objective of using radar interferometry for mine highwall monitoring is twofold. First, the ability to detect movements that may be precursors to failures is required to develop an early warning system for mine workers working below unstable areas. If such a system were successful, accidents such as the one shown in Figure 8 might be avoided. Secondly, radar interferometry may provide an improved understanding of failure mechanisms. This information could be incorporated into future highwall designs by the mine's geotechnical engineering staff.



Figure 8. Drill cab crushed and operator fatally injured from highwall failure at open pit mine. Photo from Mine Safety and Health Administration (MSHA, 1998).

Radar interferometry can be applied to highwall monitoring in one of two identified approaches. In the first approach, a single, two-dimensional scanning antenna is used to sweep the highwall face. This is the approach used by the Australian slope monitoring radar discussed in previous chapters and is illustrated in Figure 9 (Potts and Noon, 2003, and Reeves, 1997). At each scan location a radar signal is transmitted, and the radar echo is received and processed. The radar phase at each scan location is then compared to phase data from previous scans.

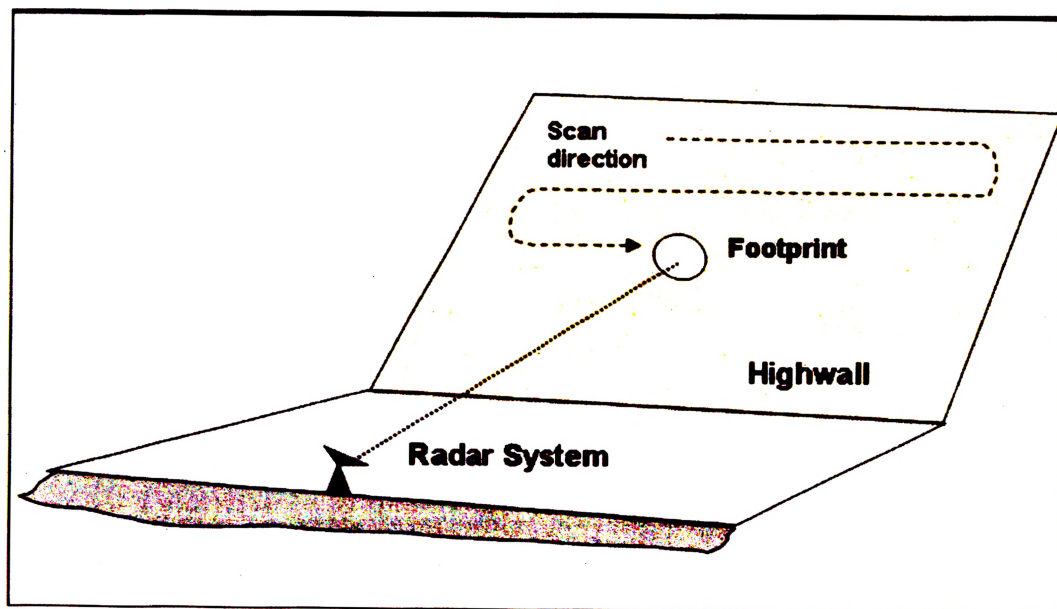


Figure 9. Principles of operation of the radar highwall monitor developed by Australian researchers. Illustration adapted from Reeves et al. (1997).

The second approach (possible using the BYU interferometric radar) involves using one transmitter and two receivers configured for either azimuth interferometry or range interferometry. In this scenario, two fan-beams scan along the highwall and illuminate the entire vertical face over a narrow horizontal width (Figure 10). The interferometric phase difference between the antennas is recorded for each scan position.

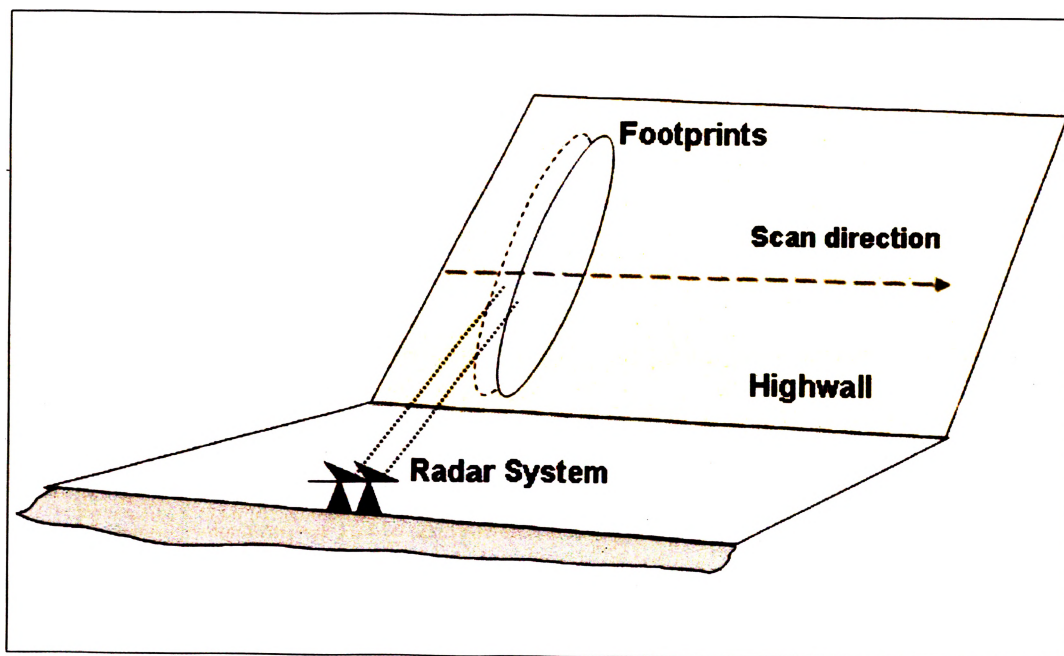


Figure 10. Principles of operation of BYU radar applied to highwall monitoring. (Adapted from Long , 2003).

Basically as a radar signal is sent to the highwall face, the return signal (echo) is used to compute the path length between the radar position and the sampled portion of the highwall. Any changes in the path length are assumed to be due to the movement of the highwall face. Since the radar is stationary, the differential interferometric phase

between scans can be easily computed. The differential phase is very sensitive to change in the plane of the baseline orientation, and the phase difference between the two interferograms can be used to calculate the displacement within the radar footprint.

3.1.3 Radar Field Experiments. For demonstration purposes, the BYU radar system was tested in a series of simple experiments at a sand and gravel pit near Provo, Utah. The prototype instrument is located near the van approximately 30 m (98 ft) from the base of the gravel pile (Figure 11 left side). The gravel slope was used for controlled slope failure experiments. Ideally, long-term tests on a cut slope or operating mine highwall would have been a better alternative; however, the gravel slope allowed easy access and was close to the research university. In addition, this site provided a straightforward means for quickly and easily creating both small and large slope displacements.



Figure 11. View of field experiment site for BYU radar.

Figures 12a and 12b provide a closer view of the test site and the view from the instrument location, respectively. The gravel pile shown in the photo is approximately 11 m (36 ft) high and has a slope of approximately 35 degrees. To establish a baseline the radar was directed toward the undisturbed slope, and the information was recorded for several minutes. Data were then recorded while one of the researchers climbed up, and then back down, the gravel pile. This simple test provided gross movements in a known direction in the radar scene and was used to ensure the instrument was properly recording and processing information from the target (actual results are discussed in Chapter 4).



Figure 12a. View of the experimental site. Gravel pile used to simulate a mine highwall.



Figure 12b.

View of test target from the radar instrument location.

3.2 SPECTRAL IMAGING

3.2.1 Imaging Spectrometer Prototype Specifications. The prototype instrument used for the multi-spectral imaging tests was a spectro-polarimetric imager developed at CMRI (Denes et al., 1998). The instrument, shown in Figure 13, is capable of obtaining multi-spectral images in the visible and near-infrared ranges. The all-electronic imager was originally built for military target recognition and utilizes an acousto-optic tunable filter (AOTF) along with a liquid crystal variable retardation plate to rapidly adjust parameters for high frame rates (Gupta et al., 1999; Denes et al., 1998).

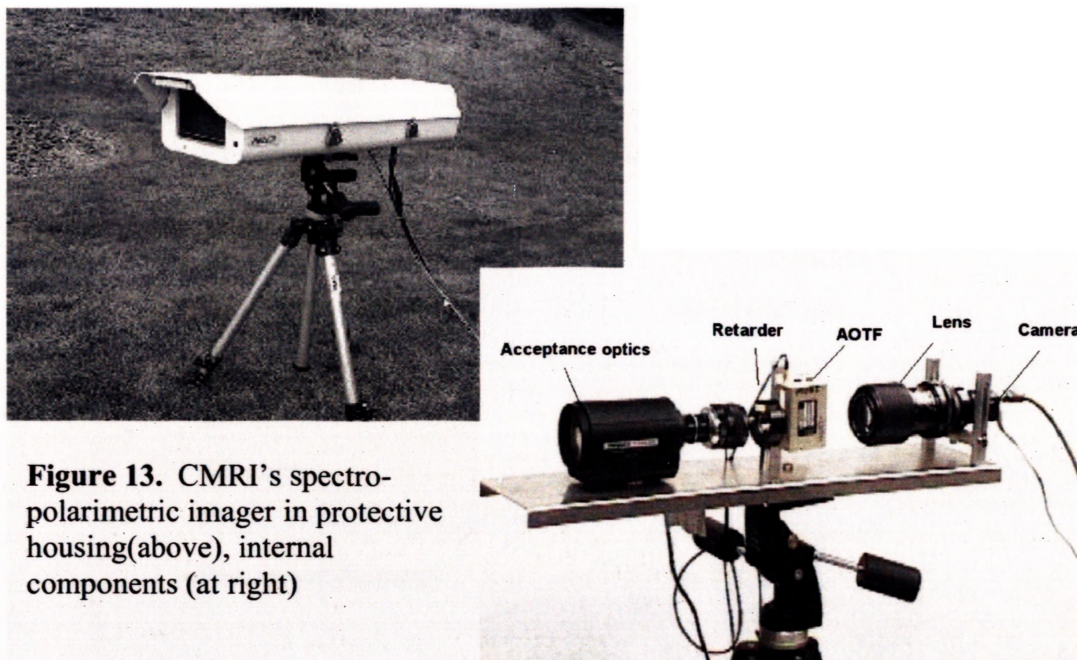


Figure 13. CMRI's spectro-polarimetric imager in protective housing(above), internal components (at right)

Other components of the imager include radio frequency (RF) electronics, image-forming optics, a charge-coupled device (CCD) camera, and an external control computer with a frame grabber video board and processing software. A summary of the imager specifications are listed in Table 3. The instrument is compact and field-portable and offers tremendous flexibility for quickly obtaining images in a variety of environments.

3.2.2 Prototype Principles of Operation. Established hyperspectral imaging systems, such as AVIRIS mentioned in Chapter 2, are based on conventional diffraction gratings and prisms with two-dimensional detector arrays (Rickard et al., 1993, and Porter and Enmark, 1987). To build an image, such systems operate in “whiskbroom” or

Table 3. CMRI spectro-polarimetric imager specifications (McHugh et al., 2001)

Parameter	Value
Spectral range	450-1000 nm
Switching rate	30 microsec/band
Retarder range	400-1800 nm
AOTF aperture	15×15 mm
RF range	25-60 MHz
RF power	<1 W
Field of view (adjustable)	1.6 to 16 degrees
Power requirement	110 V, AC

“pushbroom” mode to collect data in hundreds of narrow spatial bands. CMRI’s AOTF-based imaging system samples an entire two-dimensional scene at once without the need for moving parts. This operational mode makes the instrument compact, robust, and light-weight as compared to heavy, bulky airborne systems. The imaging capability of the instrument is also a tremendous advantage over currently available hand-held spectrometers that sample on a point-by-point basis.

The wavelength of the instrument is selected by tuning the applied RF frequency that interacts with the AOTF. The spectral range, spectral bandwidth, and polarization parameters can be controlled by the software in the host computer. Two control modes—

sweep mode and switching mode—can be used at 30 microseconds per spectral band over the wavelength range from 450-nm to 1000-nm. In sweep mode, the AOTF sequences through the full spectral range of the instrument, collecting the maximum amount of information in a scene. In switching mode, the instrument alternates between a set of very specific parameter settings for quick collection of explicit wavelengths from the sampled scene. As the instrument cycles through the various spectral bands, data cubes (Figure 14) are generated that can be processed by standard hyperspectral analysis software.

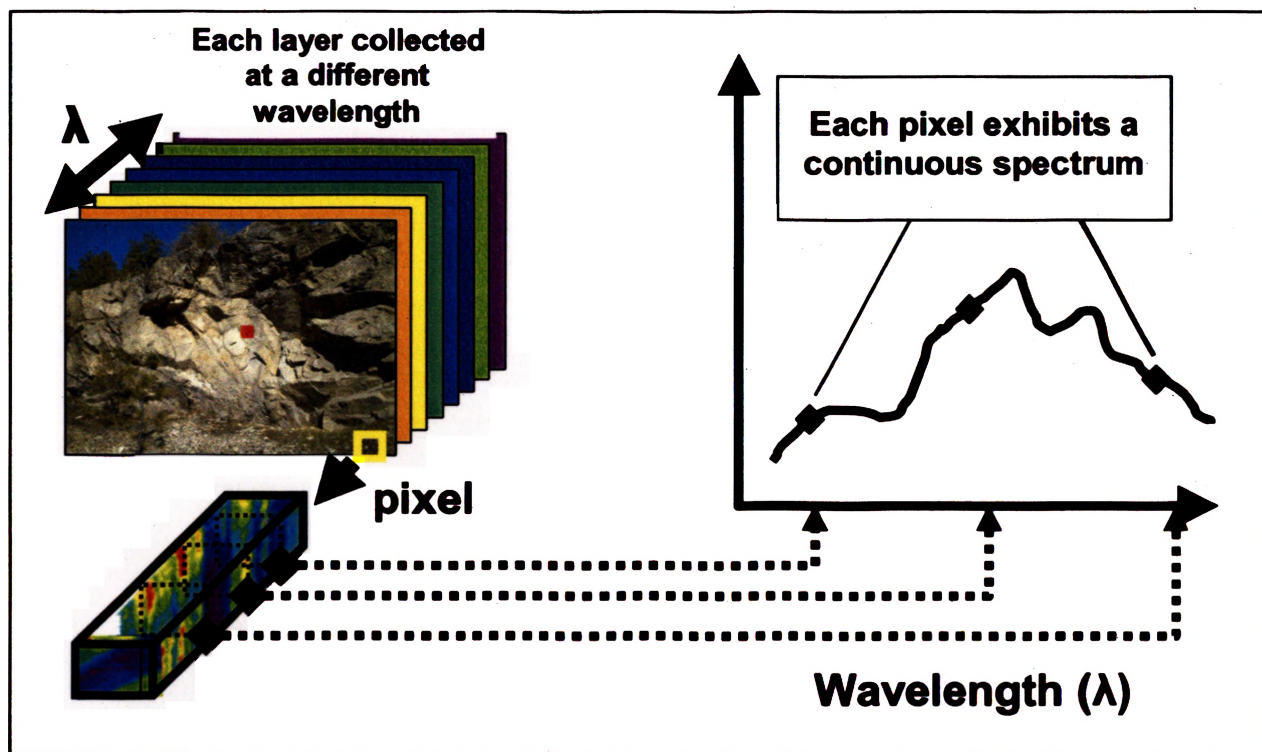


Figure 14. Image cube formed by accumulation of spectral data.

3.2.3 Multi-Spectral Imaging Field Experiments. Twelve multi-spectral images, including pit highwalls, outcrops, drill core, and hand samples, were collected from an open pit mine in southern California (Figures 15a through 15d). Data were collected from 47 bands in 10-nm intervals from 480 to 940 nm. For each scene, 190 bitmap files of original raw data were compiled into data cubes using Environment for Visualizing Images (ENVI™) software. This image-processing software provides analysis and visualization tools for single-band, multi-spectral, and radar remote-sensing data.

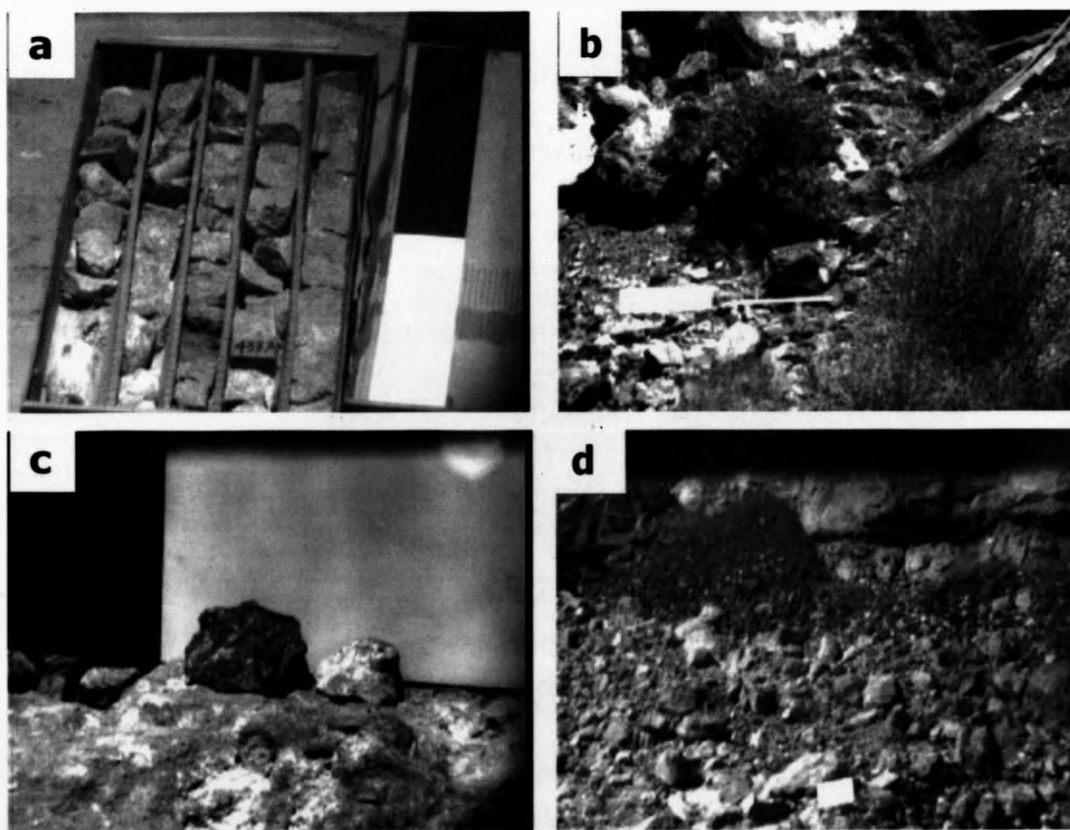


Figure 15. Original images from CMRI spectro-polarimetric imager: a) drill core; b) vegetation and outcrop; c) hand samples; and d) wall in main pit.

A number of steps were taken to ensure that the CMRI instrument was returning proper results. Original images were 640x480 pixels in size before being cropped to eliminate dark margins around the perimeter. Examples of the dark borders can be seen in the original photos in Figures 15a through 15d. The dark edges are artifacts of the lens cover and do not provide information about the target image. In each analyzed scene solid black card and solid white cards were used to correct for path radiance and to normalize the relative reflectance of the data. Examples of these cards can be seen in the rightmost portion of Figure 15a. Supplemental images of hand specimens under various light sources were collected at CMRI, and geologic thin sections were made from both ore and host rock. Redundant measurements of these mineral specimens were made using an Analytical Spectral Devices (ASD) point spectrometer, and this information was further used to test and calibrate the CMRI instrument. Figure 16a shows an example of a

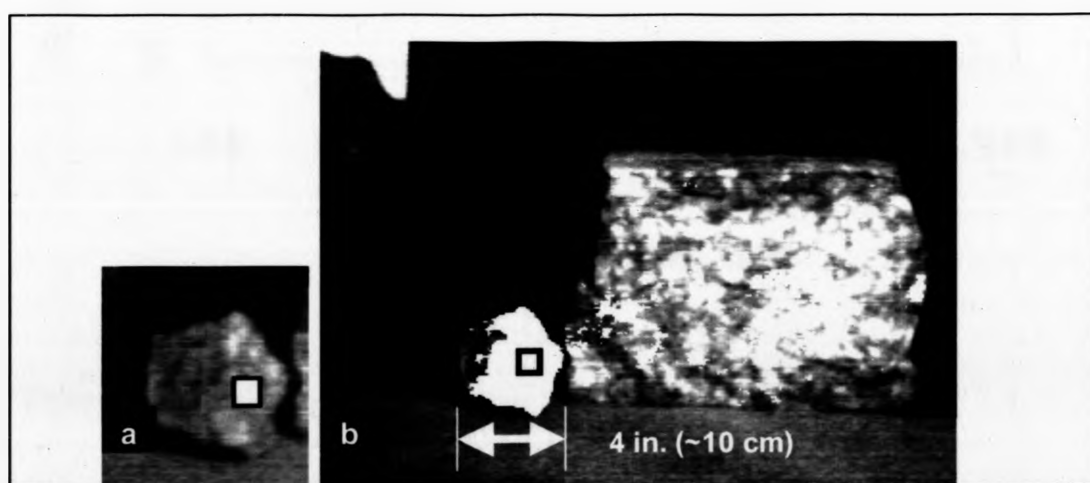


Figure 16. Laboratory calibration a.) hand specimen that was used to calibrate the CMRI imager; b) image from CMRI spectrometer on sample and larger specimen.

hand sample that was analyzed with the point spectrometer; the calibrated image using the CMRI spectral imager is shown for the sample and a larger specimen in Figure 16b. Figure 17 shows a comparison of the ASD spectrometer with the CMRI imager. More images and field results are presented in Chapter 4.2.

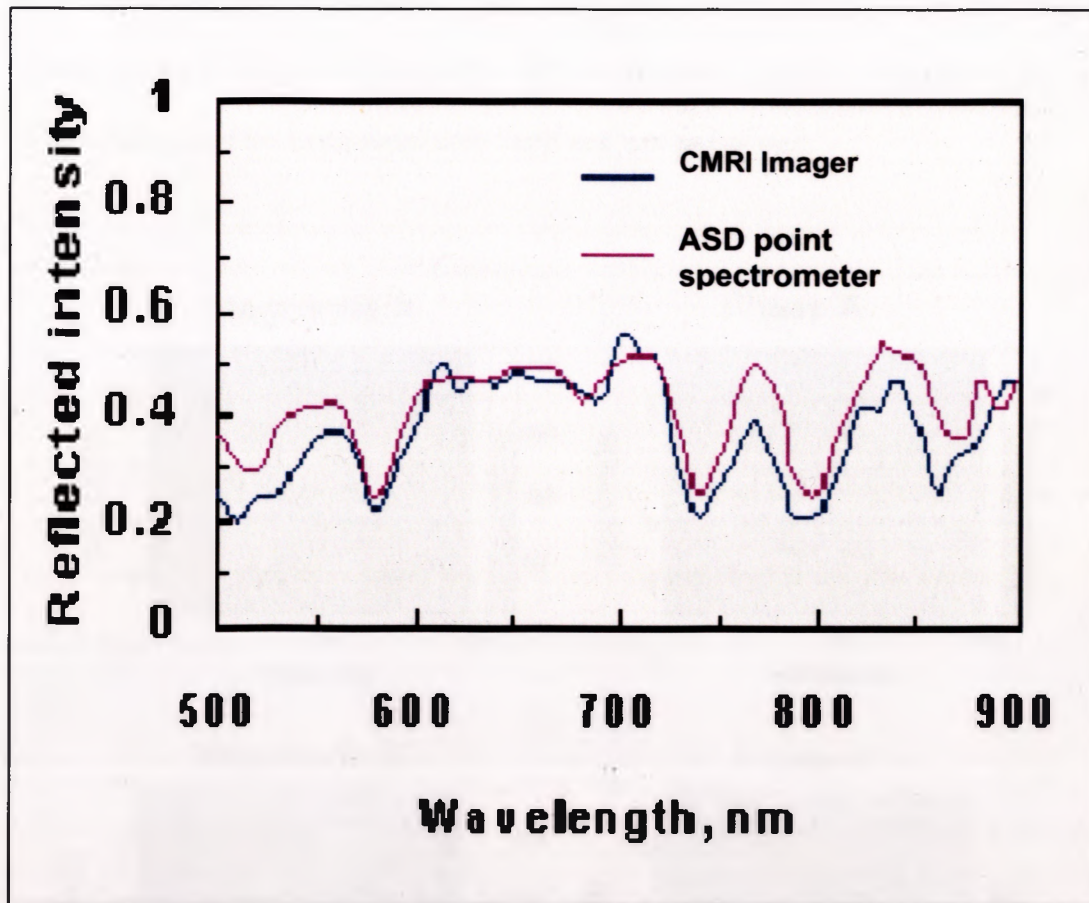


Figure 17. CMRI imager results versus ASD point spectrometer.

4. TEST RESULTS AND DISCUSSION

4.1 RESULTS FROM RADAR TESTS

In Figure 18, the baseline data for the radar interferometry tests are shown. The magnitude (in decibels) and the recorded phase for antenna A and antenna B are shown as a time series for 10 seconds. The lines that appear around 30 to 40 meters are reflections from the gravel slope. The differences shown around zero meters are caused by interference of the instrument with itself and can be ignored.

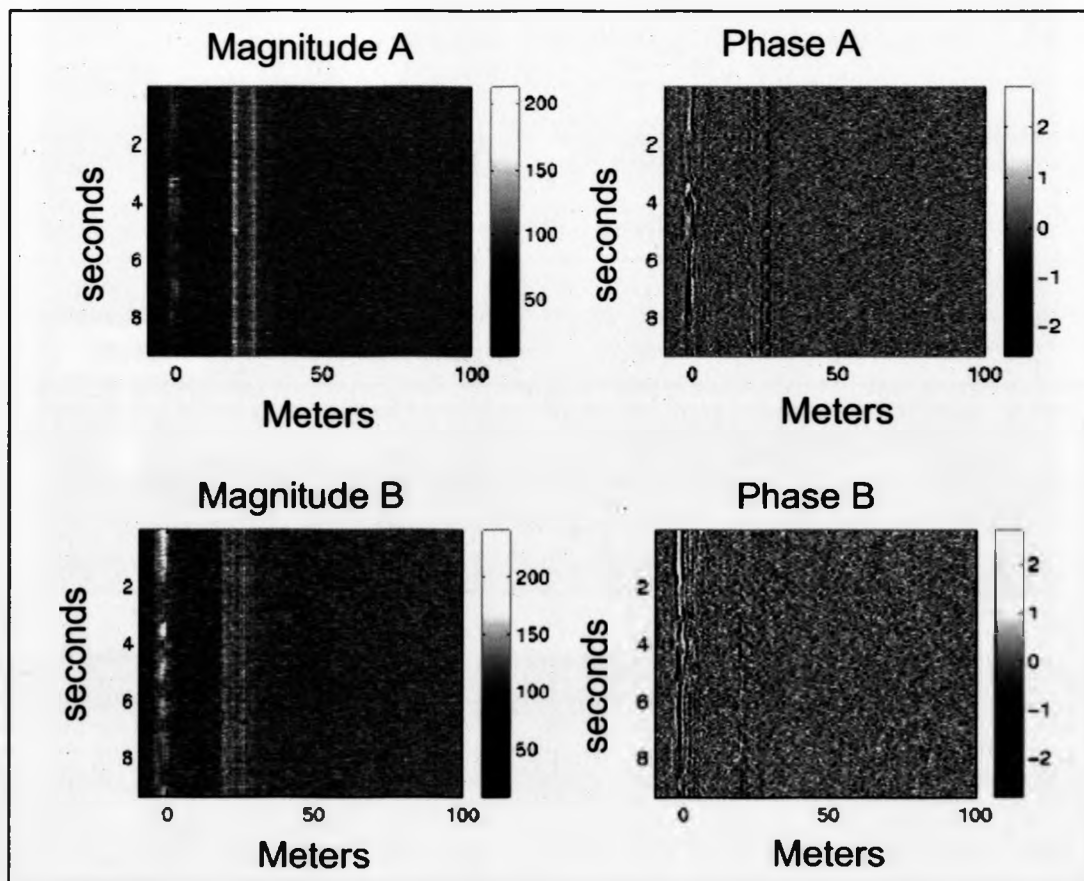


Figure 18. Baseline radar readings for each radar antenna.

Once a good baseline was established, a test of gross movement in a known direction was achieved by recording the motion of a person climbing up and down the gravel slope and displacing gravel (Figure 19). Information from each of the radar receiving antennas was recorded as the person moved throughout the scene; this information was used to monitor the resulting disturbance in the gravel.

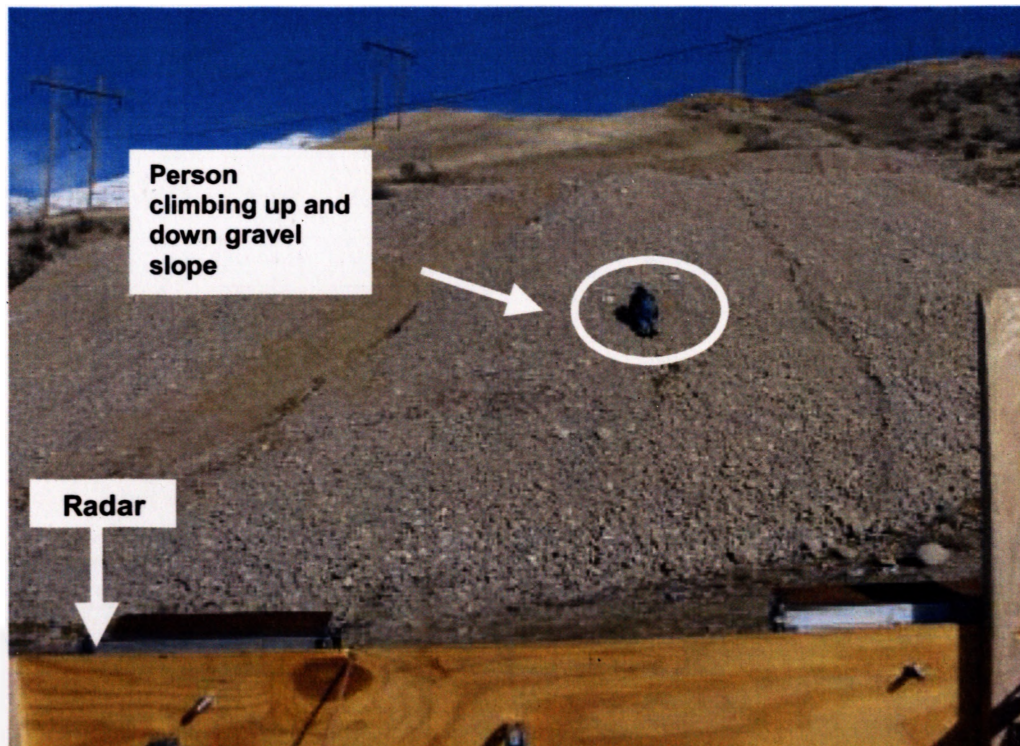


Figure 19. Large displacements in known directions were recorded as a person climbed up and down the gravel slope within the radar scene.

The individual channels are illustrated in Figure 20 as a function of time. Since the radar was stationary and did not scan across the gravel slope, these are not images of the entire scene. The images in the figures represent time records from a single scan slice of the radar looking toward the slope. Although differences in magnitude and phase are apparent in these images, information about whether the slope is deforming is derived from comparing the phases from antenna A and antenna B.

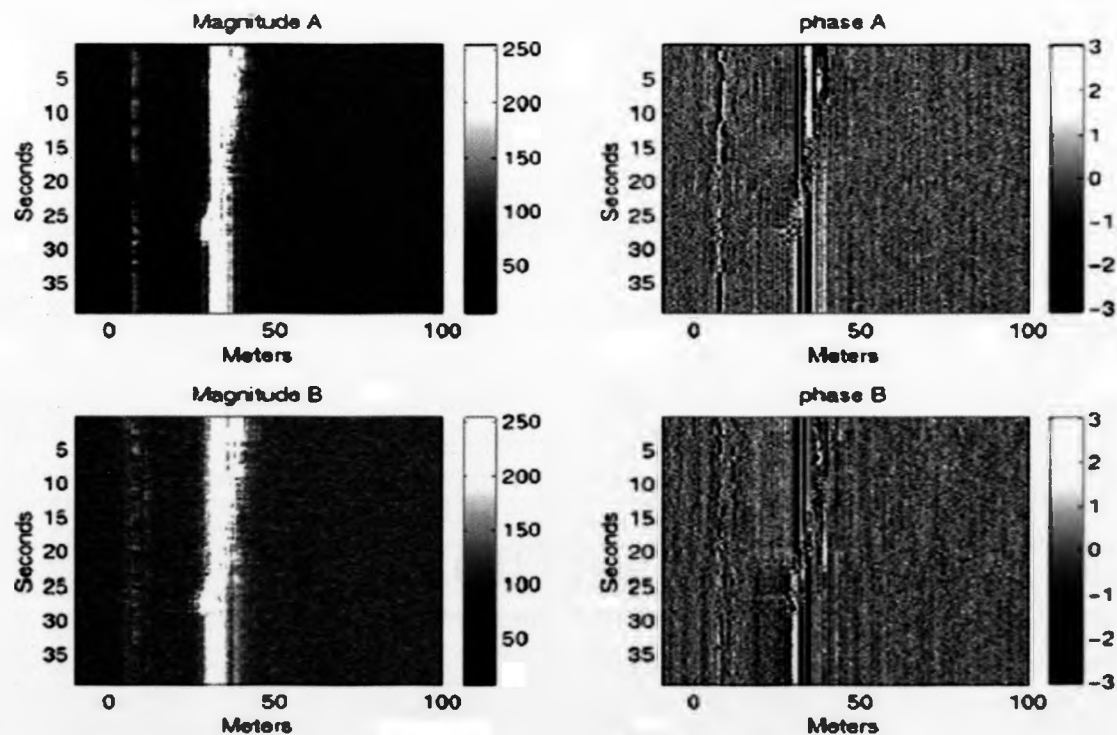


Figure 20. Raw data from each radar receiver during climbing tests

Figure 21 shows the phase difference information between radar A and radar B. Information is plotted every 0.05 seconds. As can be seen from this figure, the radar system is obviously detecting a disturbance and shows the direction of movement from the top of the slope (around 40 m) to the bottom of the slope (around 30 m).

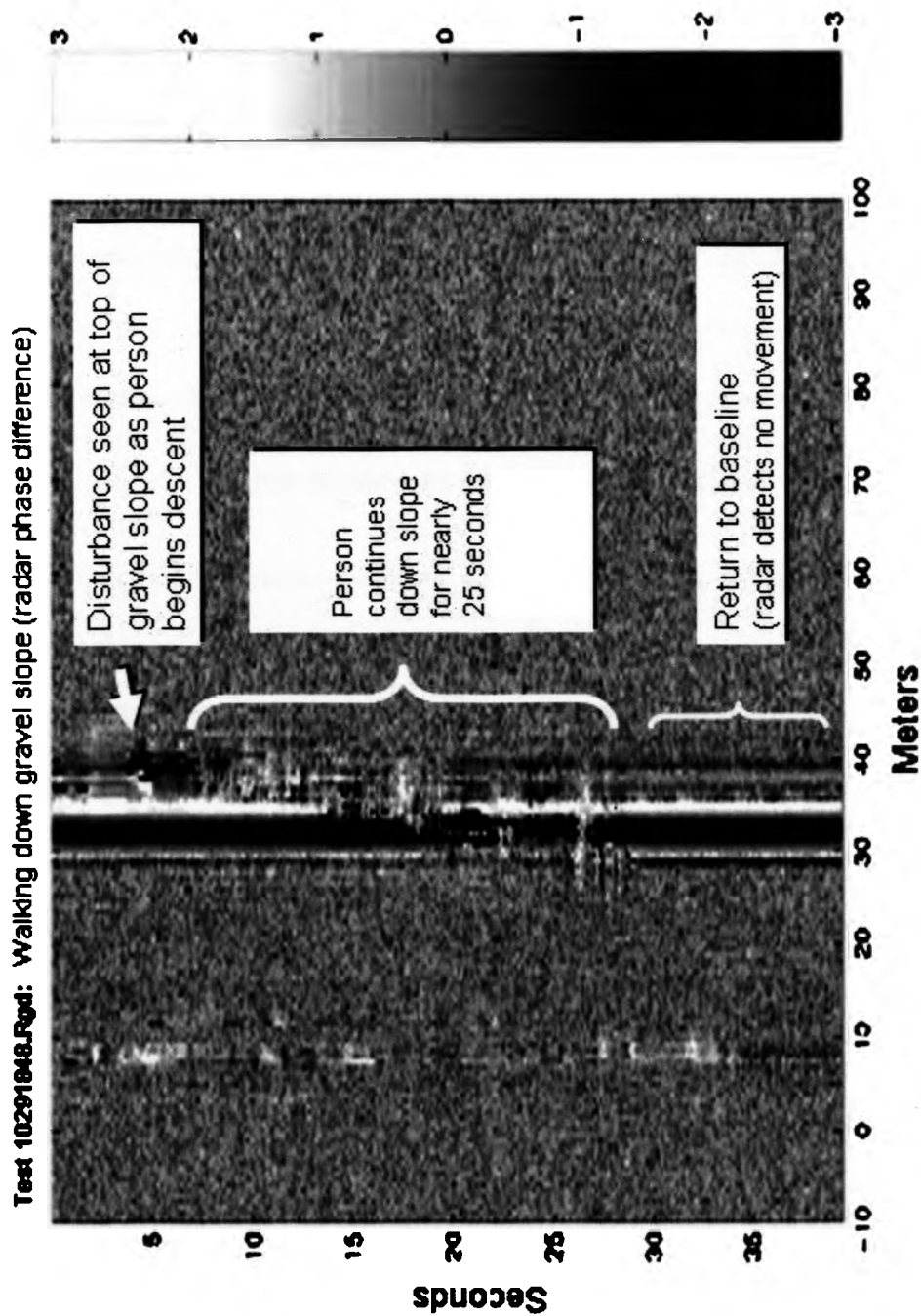


Figure 21. Radar phase difference data of person walking down gravel slope. Note direction of movement is apparent (from top of slope near 40-m down to bottom of slope around 30-m).

For this experiment, BYU provided images such as the one as shown in Figure 21, but did not provide numeric data. In order to assign numeric values to the data, the following process was used. The value of the phase change (as shown by the rightmost scale in Figure 21) is between -3 and 3 radians (0 to 2π) and encompasses the entire range of the gray-scale colors from 0 to 255 . Using standard image processing software, each pixel in the study region was assigned a corresponding darkness number (D_n). For example, if a pure white pixel was picked, the value corresponded to a darkness number of 255 , and a phase change in radians of $+3$. Conversely, if a pixel were pure black, the assigned darkness number became zero, and the phase change was recorded as -3 radians. Using this relationship, every phase change value between -3 and $+3$ radians could be correlated with the darkness number in the image using the following relationship:

$$\text{Phase change (in radians)} = (D_n - 127) + 42 \quad [1]$$

This method was time-consuming and labor-intensive, but provided a reliable means for assigning values to the data images.

In order to analyze the amount of displacement that occurred, a small region was selected for study as indicated by the box in Figure 22. An enlarged view of this study area is shown in Figure 23. To begin analysis of displacement for this data set, the difference between each adjacent pixel was computed over the time-period indicated by the vertical line in Figure 23. The time interval between data points was approximately 0.05 seconds, so the interval from 17.45 seconds to 23.14 seconds contained 108 data points. The raw data is included in an Appendix at the end of this document..

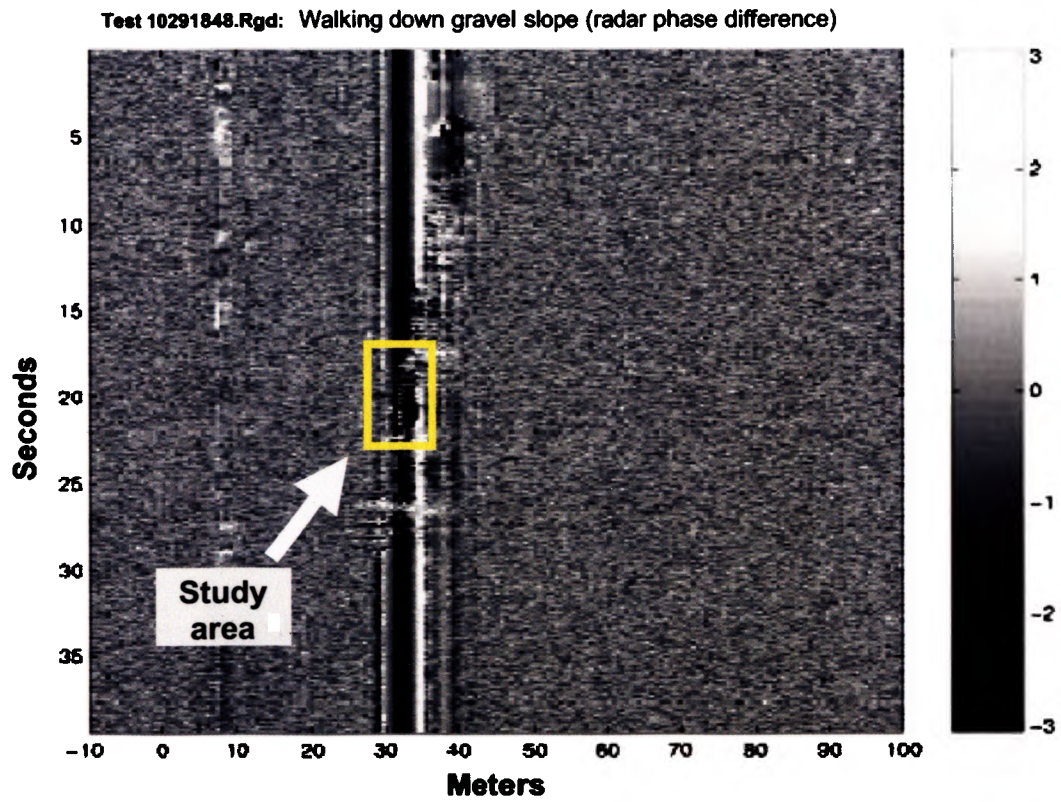


Figure 22. Box indicates analysis region. (Same data as Figure 21 was used).

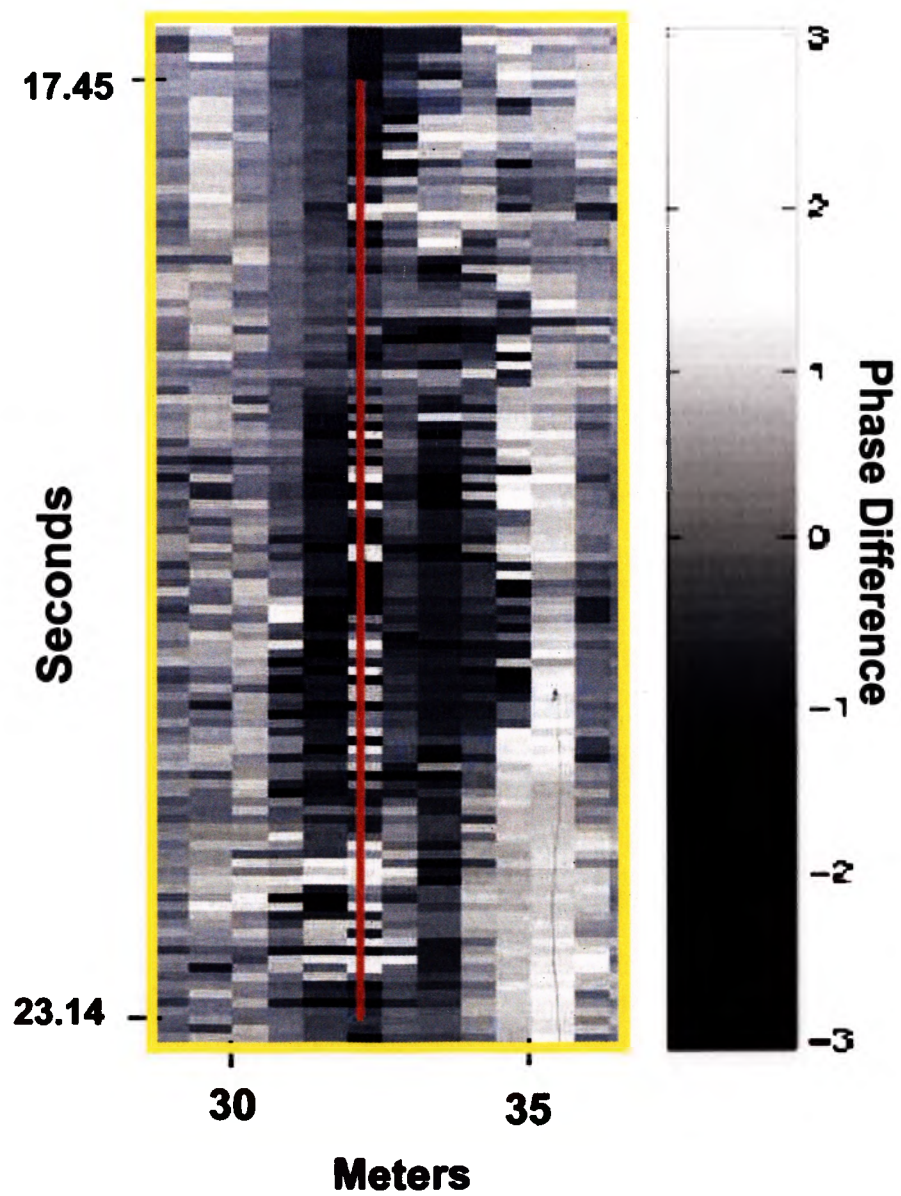


Figure 23. Enlarged view of study area indicated in Figure 22.

For interferometric radar with separate transmitters and receivers, the displacement is related to the phase change by the following formula:

$$\Delta d = ((\Delta\Phi) \lambda) \div 2\pi, \quad [2]$$

where Δd is the change in displacement (cm), $\Delta\Phi$ is the phase change in radians, and λ is the wavelength of the radar (cm). The wavelength of the BYU 9.9 GHz radar is 3.03 cm. To compute the amount of displacement that occurred from one pixel to the next, the difference in the darkness numbers was found so that the phase change in radians could be computed. The phase change information was then used to compute the displacement.

For example between 17.45 seconds and 17.50 seconds, the darkness number changed from 25 to 40. This corresponds to a phase difference of 0.36 radians. Using equation 2, the net displacement between those two pixels is computed as:

$$d = ((0.36) * (3)) / 2\pi$$

or,

$$d = 0.17 \text{ cm (0.07 in).}$$

In this data set, such a low displacement number can most likely be attributed to noise. Larger phase differences, and therefore larger displacements, occur later as the person walks through the region of interest. For example, from 18.30 seconds to 18.35 seconds, the darkness number changes from 177 to 9. Applying the same computation as above, this corresponds to a change in phase difference of 4 radians, and a displacement of 1.93 cm (0.76 in). The displacement for each successive pixel pair along the sample line in Figure 23 is shown in Figure 24.

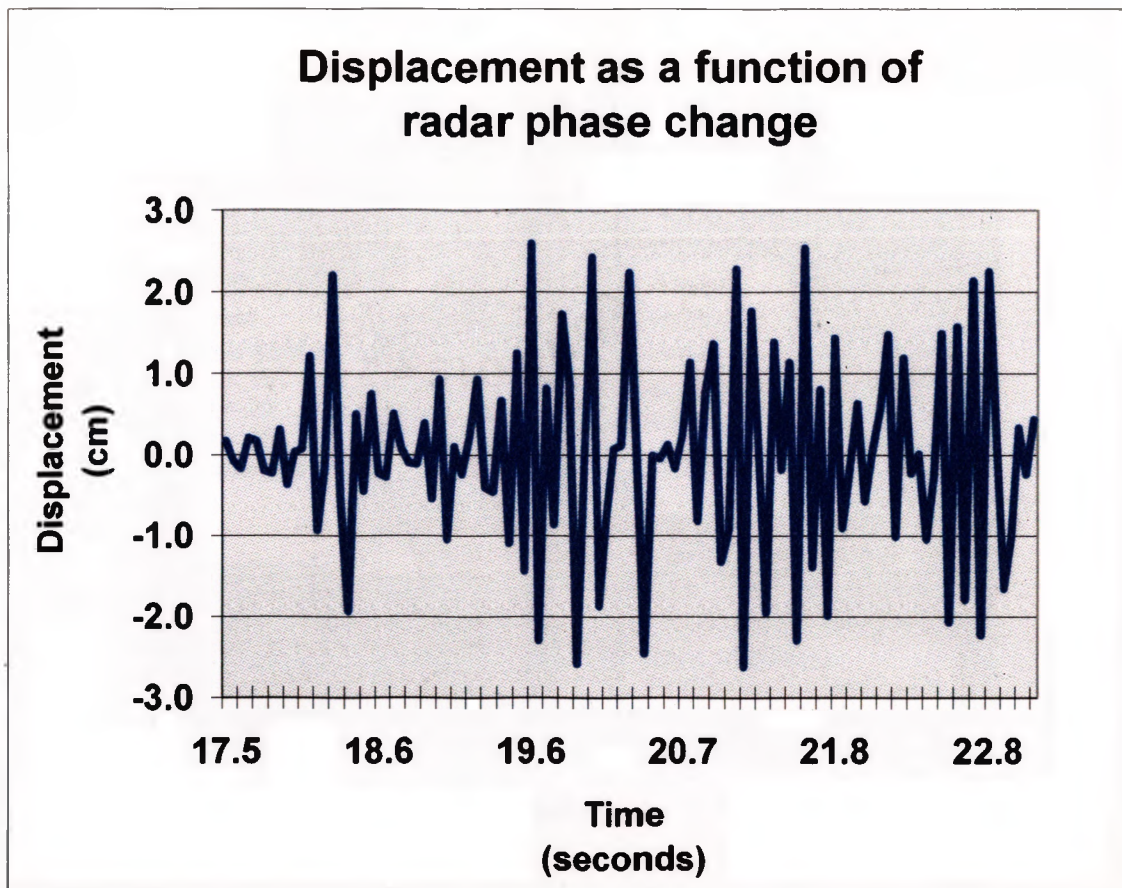


Figure 24. Net displacement for each adjacent pixel pair along the sample line indicated in figure 23.

The data analyzed in the last example only provides information about the behavior of the slope at one point. In order to extract more meaningful information, several data points along the radar footprint from approximately 30 m to 40 m (i.e., from the bottom to the top of the slope) were analyzed at times $t = 10$ sec (before person walked through radar path), $t = 22$ sec (as person walked through radar path), and $t = 28$ sec (after slope has begun to stabilize) as shown in Figure 25.

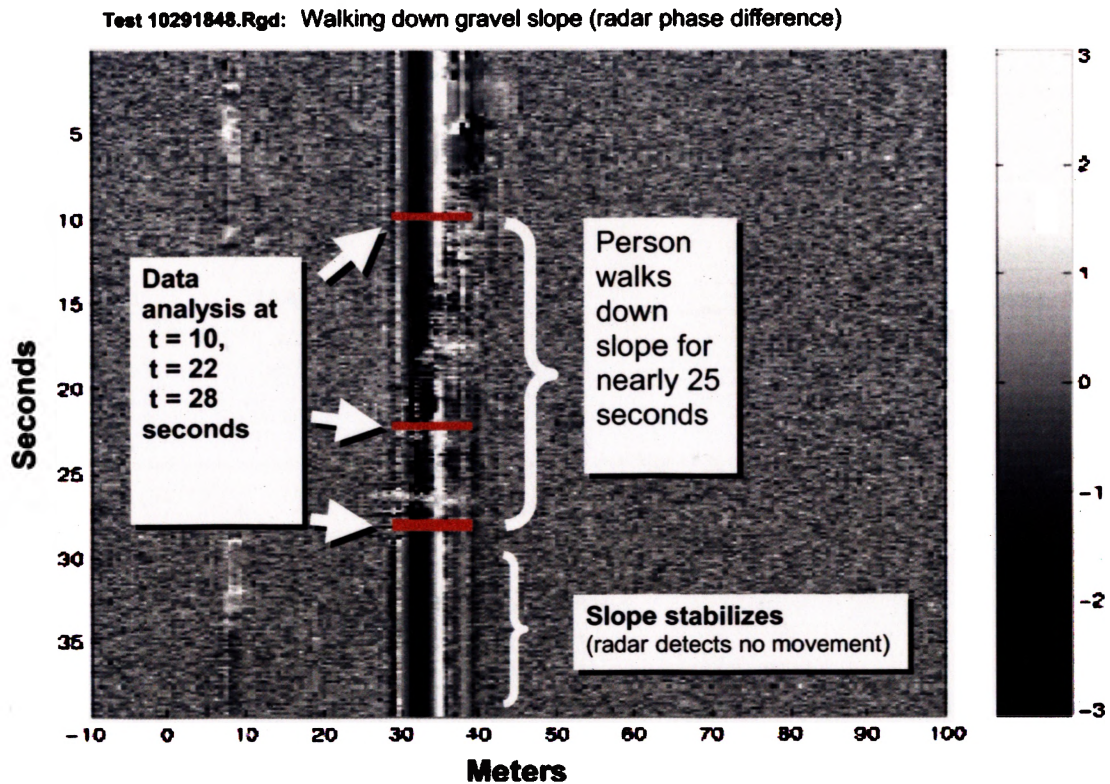


Figure 25. Data analysis along the slope profile at three separate times.

The results of the analysis are shown in Figure 26. For this example, the data at times $t = 10$ sec and $t = 28$ sec can be thought of as baseline data. In general, if there is no movement in the radar scene, the displacements will plot near zero and have a relatively flat slope. With the exception of the event that occurred near 34.7 meters at $t = 28$ sec, the displacement curves for $t = 10$ sec and $t = 28$ sec are near zero and are fairly close in agreement. Conversely, the data at time $t = 22$ sec shows displacements as high as 2.9 cm (1.1 in) in the region approximately 32 m (105 ft) away from the radar. This corresponds to a point approximately one-third of the way up the gravel slope where most of the displacement occurred.

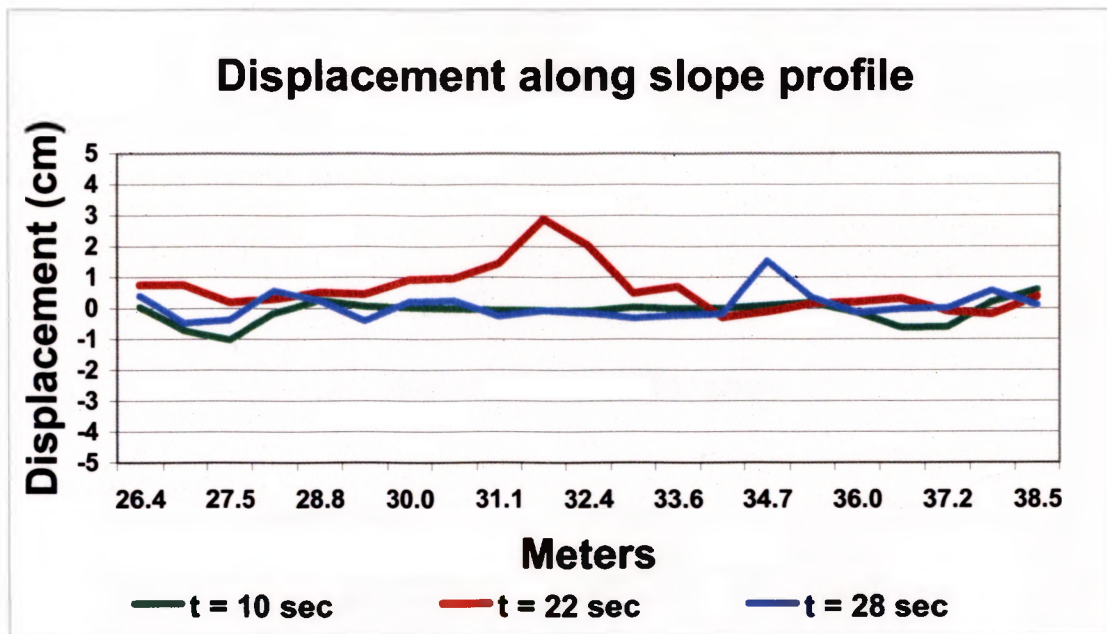


Figure 26. Results of displacement along slope profile at times $t = 10$ sec (before person walked through radar path), $t = 22$ sec (as person walked through radar path), and $t = 28$ sec (after slope has begun to stabilize).

These examples showed that it is possible to calculate slope displacements using the BYU radar data. However, the manual analysis of the data was time-consuming and tedious and would not be practical at an operating mine. In addition, a graph of a single row or column of pixels (i.e. a single radar footprint) over time does not provide adequate information for assessing the stability of the entire slope. Implementation of a scanning mechanism for the radar in order to provide multiple radar footprints would be essential. Processing software that could analyze the data and provide a two-dimensional image of the highwall, such as the one shown in Figure 27 would also need to be incorporated. Since the mathematics behind the data processing is straightforward, coding the software should be relatively simple and information on displacement, velocity, and acceleration

could all be automatically computed to assess the stability of the mine highwall. In addition, pre-processing of the radar signals to subtract noise would make it easier to quantify sub-centimeter displacements.

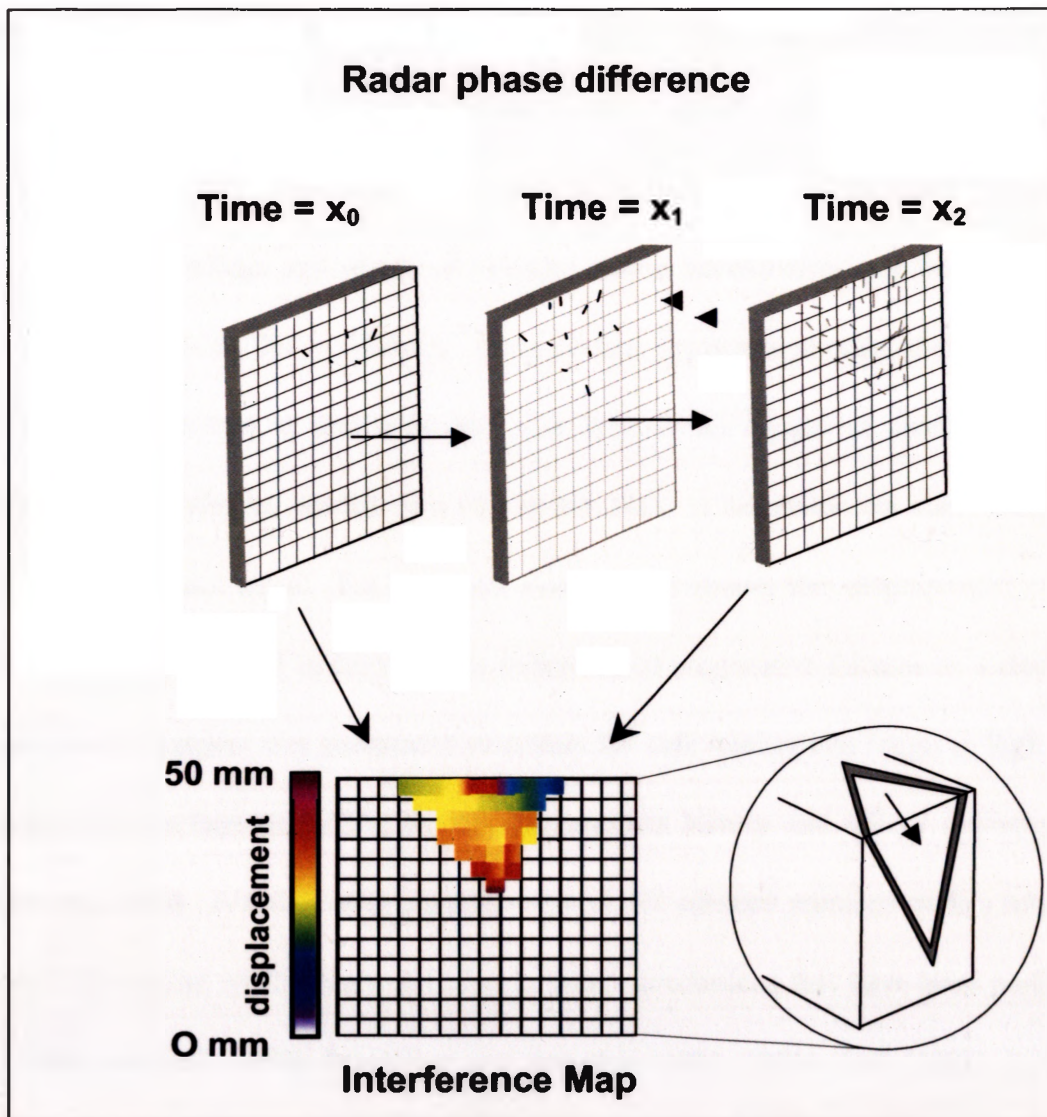


Figure 27. A displacement map could be generated by comparing phase difference information from two separate radar views of the highwall recorded at different times. [Adapted from Reeves (1997)].

The radar tests presented here were successful because they demonstrated that the prototype was capable of distinguishing centimeter-scale displacements within the radar scene. Radar interferometry is an excellent tool for detecting movement, but more research is needed to determine which (if any) of the detected displacements are potentially hazardous. Imaging radar may also provide a new means for recognizing failure modes or determining new information about slope failure mechanisms. Carefully conducted, long-term monitoring of actual mine highwalls with independently measured displacement readings and charts of velocity and/or acceleration will be essential for ultimately validating this technology. Since certain displacement rates of change may be potentially hazardous at one mine but pose little or no danger at another operation, research would also be needed on a site-by-site basis to determine the alarm sensitivity thresholds for each mine. For example, studies have shown that displacement rates in excess of 1 cm/day (0.4 in/day) may be indicative of progressive failures on a slope, but some studies suggest that acceptable velocities for safe mining can range as high as 30 cm/day (12 in/day) depending on the displacement history and failure characteristics (Zavodni, 2000). A functioning imaging radar would enhance research studies related to slope deformation mechanisms and time to failure predictions that have been performed by Ryan and Call (1992), Broadbent and Zavodni, (1982, 1978), Call (1982), Kennedy and Niermeyer (1970), and many others. Further research would also determine whether information from an imaging radar could be used to provide advance warning of small failures or rock falls.

While the experiments presented in this thesis show considerable promise for ground-based radar interferometry as a slope-monitoring tool, further research and development would be required before operational deployment became a reality. Future research issues of concern include development of methods to prevent ordinary mining operations, such as movement of equipment or personnel, from appearing as changes in the highwall. Research on the radar's long-term phase stability and effects of weather-related events such as snow and ice accumulation on benches or water running down the highwall face would also need to be tested. Unfortunately, at this time neither BYU nor NIOSH has funding to continue research and development of this instrument for highwall monitoring applications.

4.2 RESULTS FROM SPECTRAL IMAGING TESTS

As mentioned in Chapter 3, twelve multi-spectral images—including pit highwalls, outcrops, drill core, and hand samples— were collected at the site. A photo of the highwall used for the field experiments is shown in Figure 28. The box in the right side of the photo outlines the approximate region captured by the CMRI spectral imager. In the lower left portion of the box, the black cards and white cards used for calibration can be seen next to a project geologist.

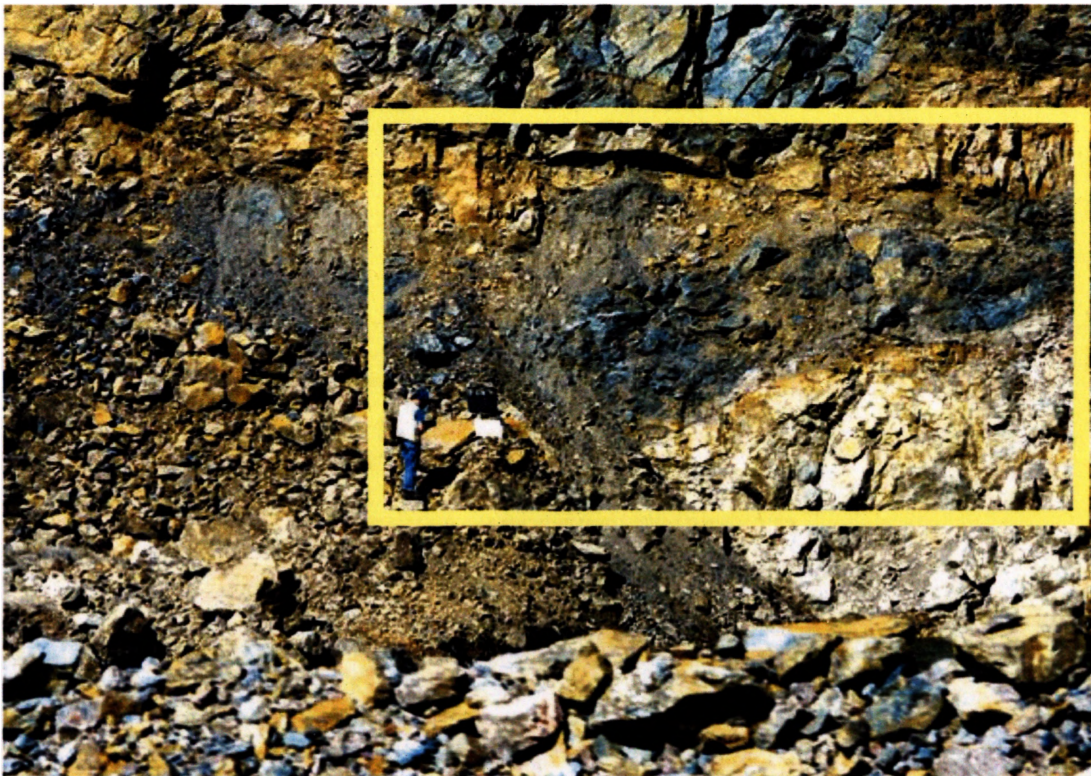


Figure 28. Mine highwall at the test site. Study area is outlined.

After the spectro-polarimetric images of the area were collected, substantial processing, filtering, and computer analyses were performed using ENVI™ image analysis software. Spectral profiles obtained in the field were compared to data in the USGS Digital Spectral Library (Clark et al. 1993) to correlate the images with specific minerals. Figure 29 illustrates the spectral signature of one of the minerals present at the mine. The spectral range of the prototype imager (480 to 1000-nm) is also indicated in the figure. Within this spectral range there are at least eight distinct spectral absorption features (points where the reflectance drops significantly) that can be used for identification; some of the most prominent features occur at approximately 520, 580, 740, 790, and 870-nm (0.52, 0.58, 0.74, 0.79, and 0.87 μm respectively).

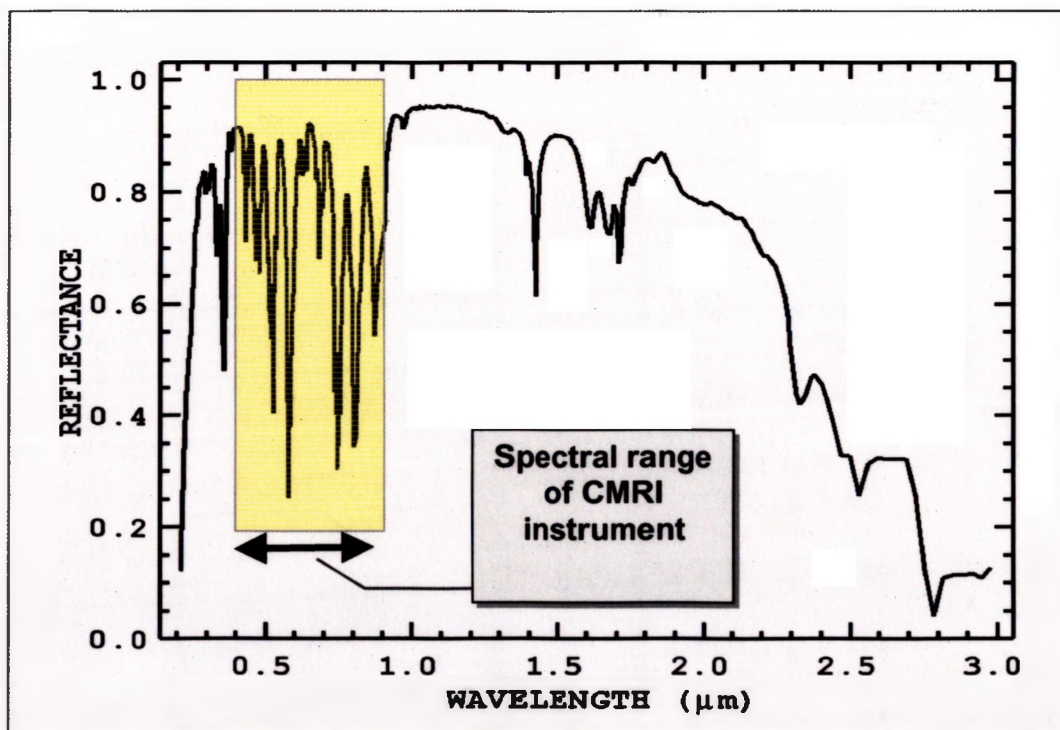


Figure 29. Diagnostic spectral signature of one of the minerals present at the field test site. The CMRI spectral operating range (480-1000 nm) is included to show that the proto-type instrument did not cover the entire spectra as published by the USGS, but did include information on at least eight distinctive absorption features (Clark et al., 1993).

Since the CMRI instrument was constrained to the spectral range from 480 to 1000-nm (0.48 to 1.0 μm), only those portions of the mineral spectra could be compared to the USGS library. Spectral reflectance and AVIRIS data for the deposit published by Rowan et al., 1986 Kingston, 1993; and Rowan et al., 1996 were also used as general guidelines for the types of spectral data and mineral assemblages anticipated at the field site. In order to analyze the spectral data obtained from the mine highwall, each pixel in the image was systematically compared to a subset of expected spectra. When spectral signatures from a pixel matched expected spectra, the pixel was classified as either “ore,” “waste,” or “unclassified.” Examples of the spectral signature between 480 and 1000-nm (0.48 to 1.0 μm) from a number of field-image pixels are illustrated in Figure 30.

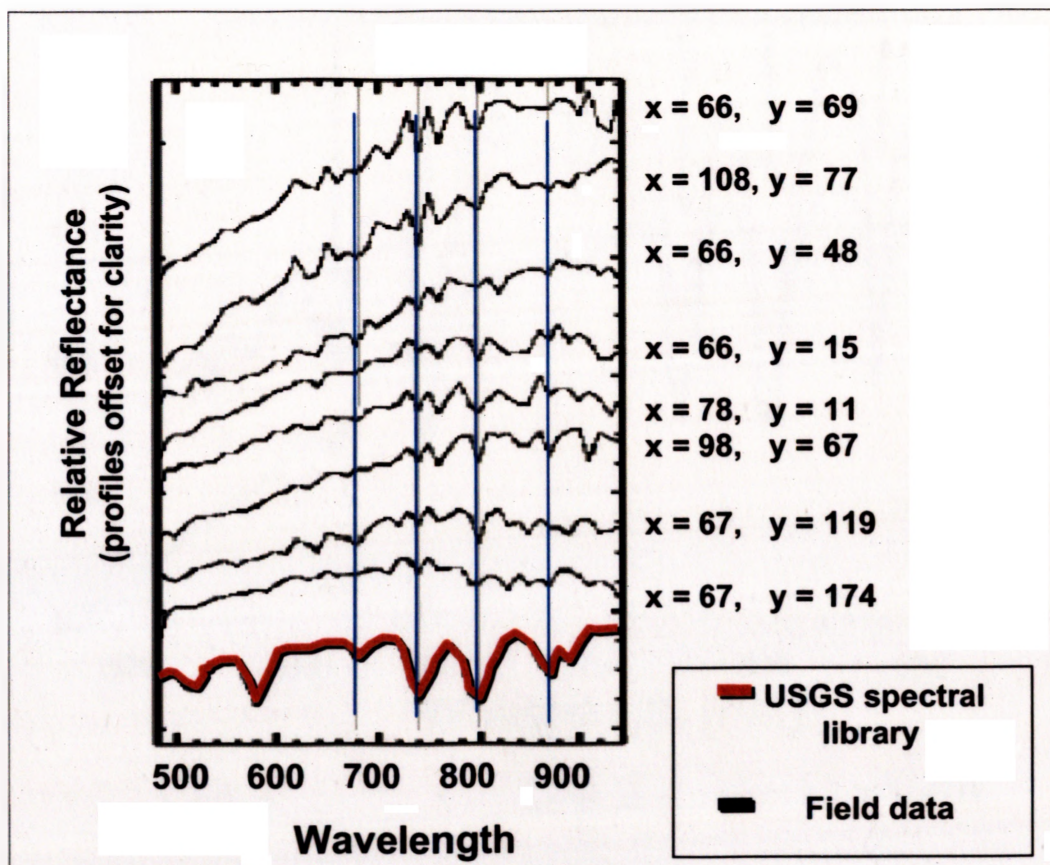


Figure 30. Comparison of spectral data.

In this figure, the expected spectral profile for one of the minerals (as determined by the ASD point spectrometer and USGS digital spectral library) is shown along with several data points extracted from various pixels throughout the image of the mine highwall. The spectral signatures are offset so that each can be viewed separately. Some of the profiles—for example pixel x:108, y:77—match nearly all the characteristic absorption features for the ore, and several correlate with the feature located near 790-nm (0.79 μm). Overall, a number of the spectral profiles correlated well with the expected mineral assemblage (Figure 31). More detailed information regarding the spectral processing can be found in McHugh et al., 2001 and McHugh et al., 2000.

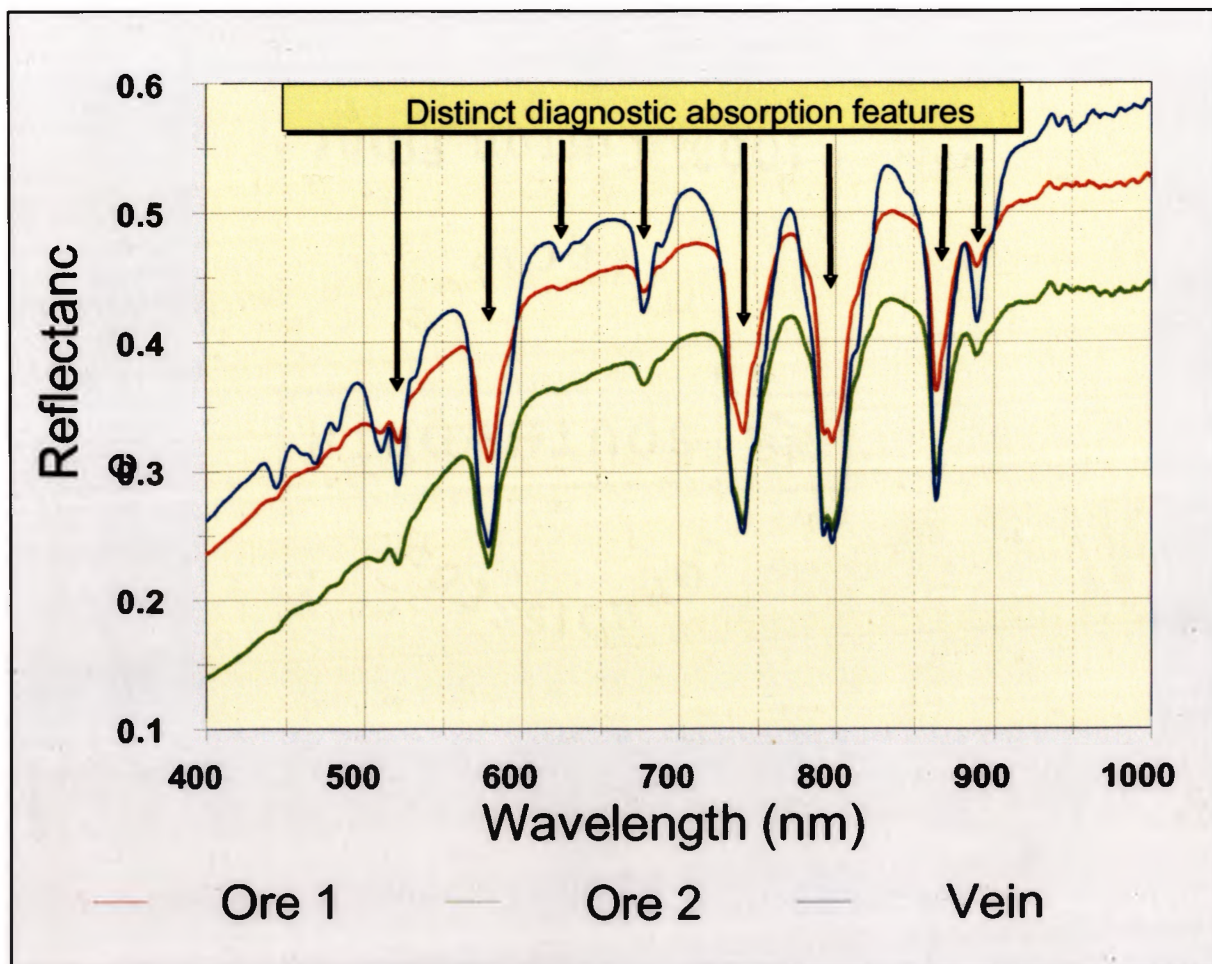


Figure 31. Spectral profiles of ore match with diagnostic absorption features.

Once every pixel in the scene was classified as ore, waste, or unclassified, the pixels were re-colored in the image to provide a visual representation of the findings. The results of the image analyses are illustrated in Figure 32. The blue areas correspond to the mine's ore, the green areas correspond to waste rock, and the black areas represent areas where the spectra were unable to be classified.



Figure 32. Results from the CMRI spectro-polarimetric imager. Blue areas correspond to ore; green areas to waste; and black to unclassified spectra.

The tests of the CMRI prototype were very successful in delineating certain minerals in the highwall. Comparisons of laboratory and field results from the CMRI imager show excellent correlation with hand-held point-spectrometer data and the USGS library data. The results from this study illustrate the capability of a field-portable imaging spectrometer to discriminate various materials within images of highwalls, outcrops, rock samples, and drill core. However, in order for the prototype instrument to be useful as a highwall monitoring tool, a redesign to extend the spectral range of the instrument is needed; particularly into the 2-2.5 μm short-wave infrared and 8-12 μm ranges where a number of clays, carbonates, and silicates can be mapped. A commercially-available, portable spectral imager could be a valuable tool for the mining industry for a number of safety, environmental, geologic, and other operational applications. At this time funding for advancement of this technology is not available at NIOSH or at CMRI.

5. CONCLUSIONS AND RECOMMENDATIONS

At this time, remote sensing cannot completely replace conventional geotechnical methods of investigation. Significant research and development of sensors, data acquisitions systems, and processing techniques is still needed. However, emerging technologies such as spectral imaging and radar interferometry should not be ignored. The satellite and/or airborne versions of these sensors have been used successfully in a number of geoscience applications such as ground subsidence, landslides, volcanoes, and fault regions. The results from the research tests presented in this thesis also provided promising results for both technologies, and the imaging aspect of both systems would serve as a tremendous advantage over systems that monitor at single points. As computer systems continue to advance and processing speeds increase, integration of remote sensing tools into mining, petroleum, civil, and environmental engineering applications will also increase.

5.1 RADAR

Even though the technological capability currently exists to build a low-cost radar system to detect displacements in a mine highwall or other rock slope, a substantial amount of creative engineering is still needed to realize a robust, working system. Methods are needed to distinguish between hazardous highwall movements and movements caused by other sources such as mining equipment. Research on the radar's long-term phase stability and effects of weather-related events such as snow and ice accumulation on benches or water running down the highwall face would also need to be tested.

Comparison of results from standard slope-monitoring systems with long-term tests of radar experiments at actual mine sites will be essential for validating the technology and determining the degree of accuracy that is required for an operation. While satellite-based radar imagers have been able to detect displacement changes of 7 mm from orbit (Massonet, 1993), further research would be necessary to determine the sensitivity levels that are not only possible, but also practical, using ground-based systems. Carefully conducted, long-term monitoring of actual mine highwalls with independently measured displacement readings and charts of velocity and/or acceleration will be essential for ultimately validating this technology. Depending on the failure characteristics, rock mass, mining configuration, and other factors, displacement rates that are regarded as hazardous at one mining operation may pose little or no danger at another; therefore, more research would be needed on a site-by-site basis to determine the alarm sensitivity thresholds for each mine. Further research would also determine whether information from an imaging radar could be used to recognize failure modes, to determine new information about slope failure mechanisms, or to provide advance warning of small failures or rock falls.

5.2 SPECTRAL IMAGING

There are many advantages to using spectral analyses for improved geologic mapping of mine highwalls. First, spectral identification of minerals would remove the human error and subjectivity of trying to visually determine the degree of alteration in a rock mass. This would enhance the safety of the mine workers since the weak areas of

the highwalls could be mapped out quickly and efficiently. Secondly, workers would be able to map large extents of mine highwalls, or inaccessible/precarious areas, from a safe distance. Spectral analyses could also be used to define faults, shear zones, and fracture systems in rock masses. All of this information could be integrated into geotechnical designs, mine planning, and mine monitoring systems.

The tests of the CMRI prototype SPI gave good results for the problem to which it was applied. Before the instrument would be functional for mine monitoring, a broader range of spectral values, particularly the range that encompasses the clay minerals that weaken mine highwalls, would be required. For the tests that were conducted, analysis of the field data was time consuming since it was done by hand. However, manual examination of the data ensured that the instrument was working properly and allowed the researchers to gain familiarity with the image processing software. This process could be automated in the future as some success in automated processing has already been shown with the USGS "Tetracorder" and "Tricorder" algorithms (Clark et al., 2002, and Swayze and Clark, 1995).

Many mining companies may view the costs of building a hyperspectral imager for mine highwall applications alone prohibitive. The CMRI estimate for expanding, modifying, and adapting a second-generation SPI exclusively for mine highwall monitoring was approximately \$70,000 (1998 U.S. dollars). However, as more research and development is completed in this field, the price could be expected to drop significantly. In addition, if properly constructed, a hyperspectral imager at a mine site could be used not only for geologic mapping, but also for mineral exploration, analysis of

tailings, pollution monitoring, reclamation, tracking the health of vegetation, toxic release inventory modeling, and many other uses.

In conclusion, a new-generation slope monitoring system consisting of an imaging interferometric radar coupled with an imaging spectrometer could provide unprecedented detail of a mine highwall. The remote-sensing nature of the instruments would allow information to be gathered remotely, without the need to send personnel into potentially hazardous areas to install equipment or to take equipment readings. Information on geology and displacements could be used to: 1) help maintain safer mining operations for personnel and equipment; 2) provide advance warning of instability to allow engineers an opportunity to modify excavation plans or minimize the impacts of a slope failure; and 3) provide information that could be used to analyze the slope failure mechanisms or determine the efficacy of remedial measures. In the future, after the appropriate research and development has been completed, costs of such a system would likely be comparable to currently existing automatic/robotic surveying systems in use today.

APPENDIX: RADAR DISPLACEMENT DATA

Time	Pixel Coordinates		Darkness Number $0 \leq D_n \leq 255$	Phase Change		Displacement (cm)	Displacement (in)
Sec	x	y	Dn	ΔD_n	Radians	$d = \lambda^*(\text{rad})/2\pi$ $\lambda = 3.03$ for BYU radar	
17.45	459	393	25				
17.50	459	394	40	15	0.36	0.17	0.07
17.55	459	395	34	-6	-0.14	-0.07	-0.03
17.61	459	396	19	-15	-0.36	-0.17	-0.07
17.66	459	397	37	18	0.43	0.21	0.08
17.71	459	398	52	15	0.36	0.17	0.07
17.77	459	399	35	-17	-0.40	-0.20	-0.08
17.82	459	400	15	-20	-0.48	-0.23	-0.09
17.87	459	401	42	27	0.64	0.31	0.12
17.93	459	402	10	-32	-0.76	-0.37	-0.14
17.98	459	403	13	3	0.07	0.03	0.01
18.03	459	404	20	7	0.17	0.08	0.03
18.09	459	405	126	106	2.52	1.22	0.48
18.14	459	406	45	-81	-1.93	-0.93	-0.37
18.19	459	407	31	-14	-0.33	-0.16	-0.06
18.24	459	408	223	192	4.57	2.20	0.87
18.30	459	409	177	-46	-1.10	-0.53	-0.21
18.35	459	410	9	-168	-4.00	-1.93	-0.76
18.40	459	411	53	44	1.05	0.51	0.20
18.46	459	412	14	-39	-0.93	-0.45	-0.18
18.51	459	413	79	65	1.55	0.75	0.29
18.56	459	414	59	-20	-0.48	-0.23	-0.09
18.62	459	415	35	-24	-0.57	-0.28	-0.11
18.67	459	416	79	44	1.05	0.51	0.20
18.72	459	417	86	7	0.17	0.08	0.03
18.78	459	418	77	-9	-0.21	-0.10	-0.04
18.83	459	419	67	-10	-0.24	-0.11	-0.05
18.88	459	420	101	34	0.81	0.39	0.15
18.94	459	421	54	-47	-1.12	-0.54	-0.21
18.99	459	422	135	81	1.93	0.93	0.37
19.04	459	423	44	-91	-2.17	-1.04	-0.41
19.10	459	424	53	9	0.21	0.10	0.04
19.15	459	425	32	-21	-0.50	-0.24	-0.09
19.20	459	426	51	19	0.45	0.22	0.09
19.26	459	427	132	81	1.93	0.93	0.37

Time	Pixel Coordinates		Darkness Number $0 \leq D_n \leq 255$	Phase Change		Displacement (cm)	Displacement (in)
Sec	x	y	D_n	ΔD_n	Radians	$d = \lambda^*(\text{rad})/2\pi$ $\lambda = 3.03$ for BYU radar	
19.31	459	428	97	-35	-0.83	-0.40	-0.16
19.36	459	429	57	-40	-0.95	-0.46	-0.18
19.42	459	430	115	58	1.38	0.67	0.26
19.47	459	431	20	-95	-2.26	-1.09	-0.43
19.52	459	432	129	109	2.60	1.25	0.49
19.57	459	433	4	-125	-2.98	-1.44	-0.57
19.63	459	434	230	226	5.38	2.59	1.02
19.68	459	435	30	-200	-4.76	-2.30	-0.90
19.73	459	436	101	71	1.69	0.82	0.32
19.79	459	437	26	-75	-1.79	-0.86	-0.34
19.84	459	438	177	151	3.60	1.73	0.68
19.89	459	439	253	76	1.81	0.87	0.34
19.95	459	440	28	-225	-5.36	-2.58	-1.02
20.00	459	441	28	0	0.00	0.00	0.00
20.05	459	442	240	212	5.05	2.43	0.96
20.11	459	443	77	-163	-3.88	-1.87	-0.74
20.16	459	444	10	-67	-1.60	-0.77	-0.30
20.21	459	445	17	7	0.17	0.08	0.03
20.27	459	446	27	10	0.24	0.11	0.05
20.32	459	447	222	195	4.64	2.24	0.88
20.37	459	448	230	8	0.19	0.09	0.04
20.43	459	449	16	-214	-5.10	-2.46	-0.97
20.48	459	450	15	-1	-0.02	-0.01	0.00
20.53	459	451	11	-4	-0.10	-0.05	-0.02
20.59	459	452	22	11	0.26	0.13	0.05
20.64	459	453	7	-15	-0.36	-0.17	-0.07
20.69	459	454	28	21	0.50	0.24	0.09
20.74	459	455	127	99	2.36	1.14	0.45
20.80	459	456	56	-71	-1.69	-0.82	-0.32
20.85	459	457	124	68	1.62	0.78	0.31
20.90	459	458	243	119	2.83	1.37	0.54
20.96	459	459	128	-115	-2.74	-1.32	-0.52
21.01	459	460	47	-81	-1.93	-0.93	-0.37
21.06	459	461	246	199	4.74	2.28	0.90
21.12	459	462	18	-228	-5.43	-2.62	-1.03
21.17	459	463	172	154	3.67	1.77	0.70
21.22	459	464	176	4	0.10	0.05	0.02

Time	Pixel Coordinates		Darkness Number $0 \leq D_n \leq 255$	Phase Change		Displacement (cm)	Displacement (in)
Sec	x	y	D_n	ΔD_n	Radians	$d = \lambda^*(\text{rad})/2\pi$ $\lambda = 3.03$ for BYU radar	
21.28	459	465	6	-170	-4.05	-1.95	-0.77
21.33	459	466	127	121	2.88	1.39	0.55
21.38	459	467	111	-16	-0.38	-0.18	-0.07
21.44	459	468	210	99	2.36	1.14	0.45
21.49	459	469	10	-200	-4.76	-2.30	-0.90
21.54	459	470	231	221	5.26	2.54	1.00
21.60	459	471	110	-121	-2.88	-1.39	-0.55
21.65	459	472	180	70	1.67	0.80	0.32
21.70	459	473	7	-173	-4.12	-1.99	-0.78
21.76	459	474	132	125	2.98	1.44	0.57
21.81	459	475	53	-79	-1.88	-0.91	-0.36
21.86	459	476	37	-16	-0.38	-0.18	-0.07
21.91	459	477	92	55	1.31	0.63	0.25
21.97	459	478	42	-50	-1.19	-0.57	-0.23
22.02	459	479	46	4	0.10	0.05	0.02
22.07	459	480	95	49	1.17	0.56	0.22
22.13	459	481	224	129	3.07	1.48	0.58
22.18	459	482	136	-88	-2.10	-1.01	-0.40
22.23	459	483	240	104	2.48	1.19	0.47
22.29	459	484	220	-20	-0.48	-0.23	-0.09
22.34	459	485	221	1	0.02	0.01	0.00
22.39	459	486	130	-91	-2.17	-1.04	-0.41
22.45	459	487	107	-23	-0.55	-0.26	-0.10
22.50	459	488	237	130	3.10	1.49	0.59
22.55	459	489	57	-180	-4.29	-2.07	-0.81
22.61	459	490	194	137	3.26	1.57	0.62
22.66	459	491	38	-156	-3.71	-1.79	-0.71
22.71	459	492	224	186	4.43	2.14	0.84
22.77	459	493	30	-194	-4.62	-2.23	-0.88
22.82	459	494	226	196	4.67	2.25	0.89
22.87	459	495	247	21	0.50	0.24	0.09
22.93	459	496	103	-144	-3.43	-1.65	-0.65
22.98	459	497	14	-89	-2.12	-1.02	-0.40
23.03	459	498	43	29	0.69	0.33	0.13
23.09	459	499	22	-21	-0.50	-0.24	-0.09
23.14	459	500	60	38	0.90	0.44	0.17

REFERENCES

- Abramson, L.W., T.S. Lee, S. Harma, and G.M. Boyce (1996). *Slope Stability and Stabilization Methods*: Chapter 8, Design, Construction, and Maintenance. John Wiley and Sons, Inc. pp. 583-620.
- Amelung, F., Galloway, D.L., Bell, J.W., Zebker, H.A., and Laczniak, R.J. (1999). Sensing the ups and downs of Las Vegas--InSAR reveals structural control of land subsidence and aquifer-system deformation. *Geology*, vol. 27. pp. 483-486.
- Asadi, J.J. and J.A. Hale (2001). A predictive GIS model for mapping potential gold and base metal mineralization in Takab area, Iran. *Computers and Geosciences*, vol. 27, no. 8. pp. 901-912.
- Asakuma K., H. Kuze, N. Takeuchi, and others (2002). Detection of biomass burning smoke in satellite images using texture analysis. *Atmospheric Environment*, vol. 36, no. 9. pp. 1531-1542.
- Barducci, A., D. Guzzi, P. Marcoionni, and others (2002). Infrared detection of active fires and burnt areas: theory and observations. *Infrared Physics and Technology*, vol. 43, no. 3-5. pp. 119-125.
- Berardino, P., M. Costantini, G. Franceschetti, A. Iodice, L. Pietranera, and V. Rizzo (2003). Use of differential SAR interferometry in monitoring and modeling large slope instability at Maratea (Basilicata, Italy). *Engineering Geology* vol. 68, no. 1-2. pp. 31-51.
- Briole, P., D. Massonnet, and C. Delacourt (1997). Post-eruptive deformation associated with the 1986-87 and 1989 lava flows of Etna detected by radar interferometry. *Geophysical Research Letters*, vol. 24, no. 1. pp. 37-40.
- Broadbent, C.D., and Z.M. Zavodni (1982). Influence of rock strength on stability. Chapter 2, *Stability in Surface Mining*, Vol. 3. C.O. Brawner (ed). Publ. Society of Mining, Metallurgy, and Exploration, Inc. pp. 7-18.
- Broadbent, C.D., and Z.M. Zavodni (1978). Slope failure kinematics. In *Proceedings of the 19th U.S. Symposium on Rock Mechanics*. Reno, Nevada.
- Brown, C.W. and G.P. Podesta (1997). Remote sensing of Coocliothophor Blooms in the Western South Atlantic Ocean. *Remote Sensing of the Environment*, vol. 60, no. 1. pp. 83-91.
- Call, R.D. and J.P. Savely (1990). Open Pit Rock Mechanics. Chapter in *Surface Mining*, 2nd edition. Society for Mining, Metallurgy and Exploration, Inc., B.A. Kennedy ed. pp. 860-882.

Call, R.D. (1982). Monitoring Pit Slope Behavior. Chapter 9, *Stability in Surface Mining*, Vol. 3. C.O. Brawner (ed). Publ. Society of Mining, Metallurgy, and Exploration, Inc. pp. 229-248.

Campbell, J.B. (1996). *Introduction to Remote Sensing*, 2nd edition. Guilford Press, New York, New York. 623 pp.

CANMET (1977). Canada Centre for Mineral and Energy Technology. *Pit Slope Manual*. Publ. 77-15, Chapter 8. 188 pp.

Carnec, C. and C. Delacourt (2000). Three years of mining subsidence monitored by SAR interferometry, near Gardanne, France. *Journal of Applied Geophysics*, vol. 43, no. 1. pp. 43-54.

Carnec, C., D. Massonnet, and C. King (1996). Two examples of the use of SAR interferometry on displacement-fields of small spatial extent. *Geophysical Research Letters*, vol. 23, no. 24. pp. 3579-3582.

Chang, S., and W. Collins (1983). Confirmation of the airborne biogeophysical mineral exploration technique using laboratory methods. *Economic Geology*, vol. 78, pp. 723-726.

Clark, R.M., G.A. Swayze, K.E. Livo, R.F. Koaly, S.J. Sutley, J.B. Dalton, R. R. McDougal, and C.A. Gent (2002). Imaging spectroscopy: earth and planetary remote sensing with the USGS Tetracorder and expert systems. *Journal of Geophysical Research*. In press. <http://speclab.cr.usgs.gov/PAPERS/tetracorder>

Clark, R.M. S. Vance, and R. Green (1998). Mineral mapping with imaging spectroscopy: the Ray Mine, Arizona. *Summaries of the 7th Annual Jet Propulsion Laboratory Airborne Earth Science Workshop*. R.O. Green (ed). JPL Publication 97-21. pp. 67-75.

Clark, R.N. and G.A. Swayze (1996). Evolution in imaging spectroscopy analysis and sensor signal-to-noise: An examination of how far we have come. *Summaries of the 6th Annual Jet Propulsion Laboratory Airborne Earth Science Workshop*. <http://speclab.cr.usgs.gov/papers/imspec.evol/aviris.evolution.html>

Clark, R.N., G.A. Swayze, A.J. Gallagher, T.V.V. King, and W.M. Calvin (1993). The U. S. Geological Survey, Digital Spectral Library: Version 1: 0.2 to 3.0 microns. U.S. Geological Survey Open File Report 93-592. 1340 pp. <http://speclab.cr.usgs.gov>

Clarke, P.J., D. Paradissis, P. Briole, P.C. England, and B.E. Parsons (1997). Geodetic investigation of the 13 May 1995 Kozani-Grenea (Greece) earthquake. *Geophysical Research Letters*, vol. 24, no. 6. pp. 707-710.

Cocks, T. (2003) Managing Director, Integrated Spectronics, Sydney, Australia. Personal communication. See also: <http://www.intspec.com>

Colesanti, C., A. Ferretti, C. Prati, F. Rocca (2003). Monitoring landslides and tectonic motions with the Permanent Scatterers Technique. *Engineering Geology*, vol. 68, no. 1-2. pp. 3-14.

Collins, W., G. Raines, F. Canney, and R. Ashley (1983). Airborne biogeophysical mapping of hidden mineral deposits. *Economic Geology*, vol. 78. pp. 737-749.

Colwell, R.N. (1956). Determining the prevalence of certain cereal crop diseases by means of aerial photography. *Hilgardia*, Vol. 26, No. 4. pp. 29-36.

Cox, D.A. (2001). USGS Groundwater and Seismic Studies Seek Common Ground through InSAR. Public affairs website article, September 4, 2001.
<http://ca.water.usgs.gov/program/desert/InSAR/bawden/>

Cunningham, C. (2001). Use of Blast Timing to Improve Slope Stability. *Slope Stability in Surface Mining*. Society for Mining, Metallurgy, and Exploration, Inc. (Publ.). Hustrulid, McCarter, and Van Zyl (editors). pp. 131-134.

Curlander, J.C. and R.N. McDonough. *Synthetic Aperture Radar Systems and Signal Processing*. New York, John Wiley and Sons. 613 pp. 1991.

Dalton, J.B., T.V.V. King, D.J. Bove, R.F. Kokaly, R.N. Clark, J.S. Vance, and G.A. Swayze (2000). Distribution of acid-generating and acid-buffering minerals in the Animas River Watershed as determined by AVIRIS spectroscopy. *Proceedings of the International Conference on Acid Rock Drainage (ICARD)*. May 21-24, 2000, Denver, Colorado.

De Rouffignac, E.P., P.L. Bondor, J.M. Karinakas, and S.K. Hara (1995). Subsidence and well failure in the South Belridge Diatomite Field. *Proceedings of the Society of Petroleum Engineers Regional Meeting*, Bakersfield, CA. pp. 153-167.

Denes, L.J., M.S. Gottlieb, S. Milton, B. Kaminsky, D.F. Huber (1998). Spectropolarimetric imaging for object recognition. *Proceedings of the International Society of Optical Engineering (SPIE), 26th AIPR Workshop: Exploiting New Image Sources and Sensors*. J.M. Selander (ed.), vol. 3240, pp. 8-18.

Dixon, T., editor (1994) SAR Interferometry and Surface Change Detection: Report of a Workshop. February 3-4, 1994, Boulder, Colorado.

Esipusu, Manoah (2001). "Rescuers dig for bodies of buried Zambia Miners." *The Namibian, Africa News Headlines*, April 11, 2001. (Website accessed Jan. 2003).
<http://www.namibian.com.na/2001/April/africa/01E63A99C1.html>

Fielding, E.J., Blom, R.G., and Goldstein, R.M. (1998). Rapid subsidence over oil fields measured by SAR interferometry. *Geophysical Research Letters*, v. 27. pp. 3215-3218.

Froger, J.L., O Merle, P Briole (2001). Active spreading and regional extension at Mount Etna imaged by SAR interferometry. *Earth and Planetary Science Letters*, vol. 187, no. 3-4. pp. 245-258.

Fruneau, B. and J. Achache (1996a). Satellite monitoring of landslides using SAR interferometry. *News Journal, International Society for Rock Mechanics*, vol. 3, no. 3.

Fruneau, B. J. Achache, and C. Delecourt (1996b). Observation and modeling of the Saint-Etienne de Tinee landslide using SAR interferometry. *Tectonophysics*, vol. 265, no. 3-4. pp. 181-190.

Gabriel, A.K., R.M. Goldstein, and H.A. Zebker (1989). Mapping small elevation changes over large areas: differential radar interferometry. *Journal of Geophysical Research*, vol. 94. pp. 9183-9191.

Galloway, D.L., Hudnut, K.W., Ingebritsen, S.E., Phillips, S.P., Peltzer, G., Rogez, F., and Rosen, P.A. (1998). Detection of aquifer system compaction and land subsidence using interferometric synthetic aperture radar, Antelope Valley, Mojave Desert, California. *Water Resources Research*, vol. 34. pp. 2573-2585.

Girard, J.M., R.T. Mayerle, and E.L. McHugh (1998). Advances in Remote Sensing Techniques for Monitoring Rock Falls and Slope Failures. *Proceedings of the 17th International Conference on Ground Control in Mining*. S. Peng (ed.) Morgantown, WV.

Girard, J.M. and E.L. McHugh (2001). Emerging Technologies and the Future of Geotechnical Instrumentation. *Proceedings of the 36th U.S. Rock Mechanics Symposium: Rock Mechanics in the National Interest*. D. Ellsworth et al. (eds.) Washington, D.C. pp. 584-591.

Goldstein, R.M., H.A. Zebker, and C.L. Werner (1988). Satellite radar interferometry: Two-dimensional phase unwrapping. *Radio Science*, vol. 23, no. 4. pp. 713-720.

Goldstein, R.M., H. Engelhardt, B. Kamb, and R.M. Frolich (1993). Satellite interferometry for monitoring ice sheet motion: application to an Antarctic ice stream. *Science*, 262, pp. 1525-1530.

Graham, L.C. (1974). Synthetic interferometric radar for topographic mapping. *Proceedings IEEE*, vol. 62. pp. 763-768.

Gupta, N., R. Dahmani, M. Gottlieb, L. Denes, B. Kaminsky, and P. Metes (1999). Hyperspectral imaging using acousto-optical tunable filters. *Proceedings of International Society for Optical Engineering (SPIE)*, vol. 3718, pp. 512-521.

Henderson, F.M. and A.J. Lewis (1998). *Principles and Applications of Imaging Radar, Volume 2: Manual of Remote Sensing*, 3rd edition. R.A. Ryerson (ed.). American Society for Photogrammetry and Remote Sensing. John Wiley & Sons, Inc. New York. 896 pp.

Hoffmann, J., Zebker, H.A., Galloway, D.L., and Amelung, F., 2001, Seasonal subsidence and rebound in Las Vegas Valley, Nevada, observed by synthetic aperture radar interferometry. *Water Resources Research*, vol. 37, no. 6. pp. 1551–1566.

Hustrulid, W.A. (1999). *Blasting Principles for Open Pit Mining, Volume 1: General Design Concepts*. Chapter 10. A.A. Balkema. pp. 293-377.

Ishiwada, Y. and Y. Akiyama (1992). Spectral approach for geologic mapping and resource exploration based on the integrated analysis of laboratory, airborne, satellite data. *Advances in Space Research*, vol. 12, no. 7. pp. 407-414.

Kennedy, B.A., and K.E. Niermeyer (1970). Slope monitoring systems used in the prediction of a major slope failure at the Chuquicamata Mine, Chile. In *Proceedings of the Symposium on Planning Open Pit Mines*. A.A. Balkema.

King, T.V.V., R.M. Clark, C. Ager, and G.A. Swayze (1995). Remote mineral mapping using AVIRIS data at Summitville, Colorado and the adjacent San Juan Mountains. *Proceedings: Summitville Forum 1995*. H. Posey et al., (eds.). Colorado Geological Survey Special Publication 38. pp. 59-63.

Kingston, M.J. (1993) Evaluation of AVIRIS data for mineral mapping at Mountain Pass, the East Mohave Desert, California. *Proceedings of the 9th Thematic Conference on Geologic Remote Sensing*, Pasadena, California. pp. 181-182.

Kliche, C. (1999). *Rock Slope Stability*. Publ. Society for Mining, Metallurgy, and Exploration, Littleton, CO. 272 pp.

Lanari, R., P. Lunedgren, and E. Sansosti (1998). Dynamic deformation of Etna volcano observed by satellite radar interferometry. *Geophysical Research Letters*, vol. 25, no. 10. pp. 1541-1543.

Li, F.K. and R.M. Goldstein (1990). Studies of multibaseline spaceborne interferometric synthetic aperture radar. *IEEE Transactions Geoscience Remote Sensing*, vol. 28. pp. 88-97.

Long, D. (2003). "Status Report Update: NIOSH Mining Hazards Interferometry Experiment." Internal Report, National Institute for Occupational Safety and Health, Spokane Research Laboratory.

Lu, Z. R. Fatland, M. Wyss, S. Li, and J. Eichelberer (1997). Deformation of New-Trident volcano measured by ERS-1 SAR interferometry, Katmai-National-Park, Alaska. *Geophysical Research Letters*, vol. 24, no. 6. pp. 695-698.

Lu, Z., C. Wicks, D. Dzurisin, W. Thatcher, J. Freymueller, S. McNutt, and D. Mann (2000). Aseismic inflation of Westdahl volcano, Alaska, revealed by satellite radar interferometry, *Geophysical Research Letters*, vol. 27. pp. 1567-1570.

Malassingne, C., F. LeMaître, P. Briole, and O. Pascal (2001). Potential of ground-based radar for the monitoring of deformation of volcanoes. *Geophysical Research Letters*, vol. 28, no. 5. pp. 851-854.

Mantovani, F. R. Soeters, and C.J. Vanwesten (1996). Remote-sensing techniques for landslide studies and hazard zonation in Europe. *Geomorphology*, vol. 15, no. 3-4. pp. 213-225.

Massonnet, D., T. Holzer, and H. Vadon (1997). Land subsidence caused by the East Mesa geothermal field, California, observed using SAR interferometry. *Geophysical Research Letters*, vol. 24, no. 8. pp. 901-904.

Massonnet, D. and K. Feigl (1995a). Discrimination of geophysical phenomena in satellite radar interferograms. *Geophysical Research Letters*, vol. 22, no. 12. pp. 1537-1540.

Massonnet, D., Briole, P., and Arnaud, A (1995b). Deflation of Mount Etna monitored by spaceborne radar interferometry. *Nature*, vol. 375. pp. 567-570.

Massonnet, D., K. Feigl, M. Rossi, and F. Adragna (1994). Radar interferometric mapping of deformation in the year after the Lander's earthquake. *Nature*, 369, pp. 227-230.

Massonnet, D., M. Rossi, C. Carmona, F. Adragna, G. Peltzer, K. Feigl, and T. Rabaute (1993). The displacement field of the Lander's earthquake mapped by radar interferometry. *Nature*, 364, pp. 138-142.

McHugh, E. (2002). "Injury analysis –Slope Stability at Surface Mines," unpublished report, National Institute for Occupational Safety and Health, Spokane Research Laboratory. Personal Communication.

McHugh, E.L., J.M. Girard, and L.J. Denes (2001). Simplified hyperspectral imaging for improved geologic mapping of mine slopes. *Proceedings of the 3rd International Conference on Intelligent Processing and Manufacturing of Materials (IPMM)*, Vancouver, British Columbia. Meech, et al., (eds.), July 29-August 2. 10 pp.

McHugh, E.L., J.M. Girard, L. Denes, P. Metes, and C. Sabine (2000). Current research on slope movement in mines: Use of hyperspectral imagery. *Proceedings of 14th International Conference on Applied Geologic Remote Sensing*, Las Vegas, Nevada, November 6-8. pp. 584-591.

Meyer, B., R. Armijo, D. Massonnet, J.B. Dechabaliér, and C. Delacourt (1996). The 1995 Grevena (northern Greece) earthquake—fault model constrained with tectonic observations and SAR interferometry. *Geophysical Research Letters*, vol. 23, no. 19. pp. 2677-2680.

Michaels, A.F. and D.A. Seigel (1996). Quantification of non-algal light attenuation in the Sargasso Sea: Implications for biogeochemistry and remote sensing. *Deep Sea Research Part II: Topical Studies in Oceanography*, vol. 43, no. 2-3. pp. 321-345.

Mine Safety and Health Administration (2000). Accident, Illness and Injury and Employment Self-Extracting Files, Part 50 Data. <http://www.msha.gov>

MSHA (1999a). Mine Safety and Health Administration, Fatal Investigation Report "Fatal Fall of Highwall, Hanson Aggregates East, Inc., Tiftonia Quarry, February 22, 1999." <http://www.msha.gov/fatals/1999/ftl99m09.htm>

MSHA (1999b). Mine Safety and Health Administration, Fatal Investigation Report "Fatal Fall of Highwall, O'Neal Quarry and Mill, October 2, 1999." <http://www.msha.gov/fatals/1999/ftl99m43.htm>

MSHA (1998). Mine Safety and Health Administrations, Fatal Alert Bulletin. "Fatal fall of rock accident, Petty's Fork Mine #1, October 5, 1998." <http://www.msha.gov/FATALS/1998/FAB98C23.HTM>

Mouginis-Mark, P.J. (1994a). Analysis of volcanic and earthquake hazards using radar interferometry. *Proceedings of the 1st Synthetic Aperture Interferometric Workshop*, Tokyo, Japan. pp. 3-6.

Mouginis-Mark, P.J. (1994b). Volcanic hazards revealed by radar interferometry. *Geotimes*, July. pp. 11-13.

Mouginis-Mark, P.J. 1995. "Analysis of Volcanic Hazards using Radar Interferometry," *Earth Observation Quarterly*, no. 27, pp. 6-10.

Mouginis-Mark, P.J., and H. Garbeil. 1993. "Digital Topography of Volcanoes from Radar Interferometry: an Example from Mt. Vesuvius, Italy," *Bulletin of Volcanology*, vol. 55, pp. 566-570.

Oriard, L.L. (1972). Blasting Effects and Their Control in Open Pit Mines in Geotechnical Practice for Stability in Open Pit Mining. *Chapter in proceedings of the 2nd International Conference on Slope Stability in Open Pit Mining*. C.O. Brawner and V. Milligan (eds). pp. 197-222.

Ozawa, S., M. Murakami, S. Fujiwara, and M. Tobita (1997). Synthetic aperture radar interferograms of the 1995 Kobe earthquake and its geodetic inversion. *Geophysical Research Letters*, vol. 24, no. 18. pp. 2327-2330.

Peltzer, G., K. Hudnut, and K. Fiegl (1994). Analysis of coseismic surface displacement gradients using differential radar interferometry: the Landers earthquake. *Journal of Geophysical Research*, vol. 99. pp. 21971-21981.

- Peltzer, G. and P. Rosen (1995). Surface displacement of the 17 May 1993 Eureka Valley, California, earthquake observed by SAR interferometry. *Science*, vol. 268. pp. 1333-1336.
- Porter, W.M. and H.T. Enmark (1987). A system overview of the airborne visible/infrared imaging spectrometer. Jet Propulsion Laboratory (JPL) Publication 87-38, pp. 3-12.
- Potts, K. and D. Noon (2003). "Slope Stability Radar," equipment brochure. GroundProbe, Pty. Ltd., Queensland, Australia. <http://www.groundprobe.com/>
- Reeves, B. (2002). Monitoring Rock Slope Deformation by Radar Interferometry. Ph.D. Dissertation, Department of Computer Science and Electrical Engineering. University of Queensland, Australia.
- Reeves, B., D. Noon, G. Stickley, and D. Longstaff (1997). Monitoring rock slope deformation by radar interferometry. *Proceedings of the Workshop on Applications of Radio Science WARS'97*, A. Kulesa (ed.) Australian Academy of Science.
- Rickard, L. J., R. Basedow, E. Zalewske, P. R. Silvergate, and M. Landers (1993). HYDICE: an airborne system for hyperspectral imaging. *Proceedings of Society of Photo-optical Instrumentation Engineers*, vol. 1937. pp. 173-179.
- Rogers, A.E.E. and R.P. Ingalls (1969). Venus: mapping the surface reflectivity by radar interferometry. *Science*, vol. 165. pp. 797-799.
- Rosen, P., S. Hensley, I.R. Joughin, F.K. Li, S.N. Madsen, E. Rodriguez, and R. Goldstein (2000). Synthetic aperture radar interferometry. *Proceedings of the IEEE*, vol. 88, no. 3. pp. 333-382.
- Rosen, P. C. Werner, E. Fielding, S. Hensley, S. Buckley, and P. Vincent (1998). Aseismic creep along the San Andreas Fault northwest of Parkfield, California, measured by radar interferometry. *Geophysical Research Letters*, vol. 25, no. 6. pp. 825-828.
- Rosen, P.A., S. Hensley, H.A. Zebker, F.H. Webb, and E. Fielding (1996). Surface deformation and coherence measurements of Kilauea volcano, Hawaii, from SIR-C radar interferometry. *Journal of Geophysical Research*, vol. 268, pp. 1333-1336.
- Rowan, L.C., R.N. Clark, R.O. Green (1996). Mapping minerals in the Mountain Pass, California, area using the airborne visible/infrared imaging spectrometer (AVIRIS). *Proceeding of the 11th Thematic Conference and Workshops on Applied Geologic Remote Sensing*, Las Vegas, Nevada. pp. 175-176.
- Rowan, L.C., M.J. Kingston, J.K. Crowley (1986). Spectral reflectance of carbonatites and related alkalic igneous rocks: Selected samples from four North American localities. *Economic Geology*, vol. 81. pp. 857-871.

Roy, D., P.E. Lewis, C.O. Justice (2002). Burned area mapping using multi-temporal moderate spatial resolution data—a bi-directional reflectance model-based expectation approach. *Remote Sensing of the Environment*, vol. 83, no. 1-2. pp. 263-286.

Ryan, T.M. and R.D. Call (1992). Application of rock mass monitoring for stability assessment of pit slope failure. In *Proceedings of 33rd U.S. Rock Mechanics Symposium*. pp. 221-229.

Sabine, C., R.T. Mayerle, J.M. Girard, D.G. Long, and P. Hardin (1999a). Use of compact interferometric radar to assess slope-movement risk in open pit mining operations. *Proceedings of the Thirteenth International Conference on Applied Geologic Remote Sensing*, vol. 1, p. 1-55.

Sabine, C., L.J. Denes, M. Gottlieb, B. Kaminsky, P. Metes, R.T. Mayerle, and J.M. Girard (1999b). A portable spectro-polarimetric imager: potential mine safety and geologic applications. *Proceedings of the Thirteenth International Conference on Applied Geologic Remote Sensing*, vol. 1, pp. 1-190-194.

Scott, A. (1996). *Open Pit Blast Design: Analysis and Optimisation*. Julius Kruttschnitt Mineral Research Centre (publ.), Australia. Chapters 4 and 9. 338 pp.

Stancliffe, R.P.W. and M.W.A. van der Kooij (2001). The use of satellite-based radar interferometry to monitor production activity at the Cold Lake Heavy Oil Field, Alberta, Canada. *American Association of Petroleum Geologists Bulletin*, vol. 85, no. 5. pp. 281-793.

Stow, R. (1997) Application of SAR interferometry to the imaging and measurement of neotectonic movement applied to mining and other subsidence/downwarp modeling. *FRINGE 96: Proceedings ESA Workshop on Applications of ERS SAR Interferometry*. Zurich, Switzerland.
<http://www.geo.unizh.ch/rsi/fringe96/papers/>

Sun, Y. P.K. Seccombe, and K. Yang (2001). Application of short-wave infrared spectroscopy to define alteration zones associated with the Elura zinc-lead-silver deposit, NSW, Australia. *Journal of Geochemical Exploration*, vol. 73, no. 1. pp. 11-26.

Swayze, G.A. K.S. Smith, R.M. Clark, S.J. Sutley, R.M. Pearson, J.S. Vance, P.L. Hageman, P.H. Briggs, A.L. Meier, M.J. Singleton, and S. Roth (2000). Using imaging spectroscopy to map acidic mine waste. *Environmental Science and Technology*, vol. 34. pp. 47-54.

Swayze, G.A. and R.N. Clark (1995). Spectral identification of minerals using imaging spectrometry data: evaluating the effects of signal to noise and spectral resolution using the Tricorder algorithm. *Summaries of the Fifth Annual Jet Propulsion Laboratory Airborne Earth Science Workshop*. R.O. Green (ed). Jet Propulsion Laboratory Publication 95-1. pp. 157-158.

Szwedzicki, T. (ed.) (1993): Geotechnical Instrumentation and Monitoring in Open Pit and Underground Mining. *Proceedings of the Australian Conference*, Kalgoorlie. A.A. Balkema (publ.). 523 pp.

Tarchi, D., N. Casagli, R. Fanti, D.D. Leva, G. Luzi, A. Pasuto, M. Pieraccini, S Silvano (2003). Landslide monitoring by using ground-based SAR interferometry: an example of application to the Tessina landslide in Italy. *Engineering Geology*, vol. 68, no. 1-2. pp. 15-30.

Thatcher, W. and D. Massonnet (1997). Crustal deformation at Long Valley caldera, eastern California, 1992-1996 inferred from satellite radar interferometry. *Geophysical Research Letters*, vol. 24, no. 20. pp. 2519-2522.

Thompson, D.G., D. V. Arnold, D. G. Long (1999). YINSAR: a compact, low-cost interferometric synthetic aperture radar. *Proceedings of IEEE Geoscience and Remote Sensing Society*. Hamburg, Germany, pp. 598-600.

Thompson and others (1999). YINSAR: a Compact, Low-Cost Interferometric Synthetic Aperture Radar. *Proceedings of the IEEE National Radar Conference*, Boston, MA. pp 221-226.

Thompson and others (1998). YSAR and YINSAR: Compact, Low-Cost Synthetic Aperture Radars. *Proceedings of the European Conference on Synthetic Aperture Radar*, Friedrichshafen, Germany. pp. 27-30.

Thompson and others (1997). YSAR: A Compact, Low-Cost Synthetic Aperture Radar. *Proceedings of Society of Photo-optical Instrumentation Engineers (SPIE)--Radar Processing, Technology, and Applications II*. Miceli (ed.), vol. 3161. pp. 2-8.

Thompson and others (1996). YSAR: A Compact, Low-Cost Synthetic Aperture Radar. *Proceedings of the International Geosciences and Remote Sensing Symposium (IGARSS)*, Lincoln, Nebraska. pp. 1892-1894.

University of Queensland (2002). "Slope Stability Radar Goes Commercial." On-line news, University of Queensland, Australia. News Release, June 26, 2002. <http://www.uq.edu.au/news/index.phtml?article=3279>

Watters, R.J., & W.D. Delahaut (1995). Effect of Argillic Alteration on Rock Mass Stability. Clay and Shale Slope Instability: Boulder Colorado, Haneberg and Anderson, (eds.) Geological Society of America Reviews in *Engineering Geology*.

Wicks, C.W., D. Dzurisin, S. Ingebritsen, W. Thatcher, Z. Lu and J. Iverson (2002) Magmatic activity beneath the quiescent Three Sisters volcanic center, central Oregon Cascade Range, USA. *Journal of Geophysical Research*. In press. Available on-line: <http://quake.wr.usgs.gov/research/deformation/modeling/papers/wicks/threesisters.html>

Zavodni, Z.A. (2000). Time-Dependent Movement of Open-Pit Slopes, Chapter 8 in *Slope Stability in Surface Mines*. W.A. Hustrulid et al., eds. Publ. Society for Mining Metallurgy, and Exploration, Inc. pp. 81-87.

Zebker, J.A. and R.M. Goldstein (1986). Topographic mapping from interferometric SAR observations. *Journal of Geophysical Research*, vol. 91. pp. 4993-2999.

Zebker, H., P. Rosen, R. Goldstein, A. Gabriel, and C. Werner (1994). On the Derivation of Coseismic Displacement Fields using Differential Radar Interferometry: The Landers Earthquake. *Journal of Geophysical Research.*, vol. 99. pp.19617-19634.

VITAE

Jami Girard Dwyer was born July 4, 1968 in Great Falls, Montana. She received Bachelor of Science degrees in Mining Engineering and Applied Computer Science from the Montana College of Mineral Science and Technology (Montana Tech) in Butte, Montana in 1992. Immediately after college she was employed by the U.S. Bureau of Mines (USBM) in Spokane, Washington where she carried out research related to rock bursts and other underground rock mechanics issues. In 1997, when the USBM was abolished, she was transferred to the National Institute for Occupational Safety and Health where she was the lead project investigator for a project related to worker safety around open pit mine highwalls. For the 2001-2002 academic year, she was a guest lecturer and taught Surveying and Mineral Economics in the University of Missouri-Rolla Mining Engineering Department.

She is a licensed professional engineer (P.E.) in the state of Washington and is a Certified Mine Safety Professional (CMSP). In addition she obtained certification as a Mine Safety and Health Administration-approved instructor for both underground and surface mine training.

Membership in societies includes the Society of Mining Engineer (SME), the National Society for Professional Engineers, the International Society of Mine Safety Professionals, the American Rock Mechanics Associations, and the International Society for Rock Mechanics. She has authored and co-authored a number of conference papers and served as the chair of the technical committee and lead technical editor for the North American Rock Mechanics Symposium (NARMS) in 2000. She is the past-president of the Columbia Section SME, a member of SME's professional registration comm current chair of publications for SME's mechanical excavation subcommittee, and a member of the Montana Tech Mining Department Advisory Board.